robotics

MDPI

Article

Event-Triggered Distributed Variable Admittance Control for Human–Multi-Robot Collaborative Manipulation

Mohammad Jahani Moghaddam [1,2,*] and Filippo Arrichiello [1]

[1] Department of Electrical and Information Engineering, University of Cassino and Southern Lazio, Via G. Di Biasio 43, 03043 Cassino, Frosinone, Italy; f.arrichiello@unicas.it
[2] Department of Electrical Engineering, Lan.C., Islamic Azad University, Student Street, Langarud 4471311127, Iran
* Correspondence: mohammad.jahanimoghaddam@unicas.it or dr.jahani@iau.ac.ir

Abstract

In this paper, we propose a distributed admittance control framework for joint manipulation of objects by multiple robotic arms that addresses the challenges of human–robot interaction. The system is developed to control the joint transportation of an object by N Franka Emika Panda robots (validated with up to four in simulations) using external human force estimation in a distributed manner without relying on centralized computation or force sensors. We integrate a hybrid observer by combining a distributed force estimator with a nonlinear disturbance observer (NDOB) to achieve accurate human force estimation and minimize estimation errors in simulations. Adaptive radial basis function neural networks (RBFNNs) are employed to dynamically adjust the damping and inertia parameters, enhancing the system's adaptability and stability. Event-based communication minimizes network bandwidth usage, while consensus protocols ensure synchronization of state estimates across robots. Unlike conventional methods, the proposed observer operates in a fully sensorless manner: no human-force measurements are required. The estimation relies solely on locally available robot states, maintaining high accuracy while reducing system complexity. The framework demonstrates scalability to multiple robots, enhancing robustness in distributed settings. Simulation results show superior performance in terms of path tracking, force estimation accuracy, and communication efficiency compared to centralized approaches. Specifically, the event-triggered strategy reduces communication messages by approximately 70% compared to always-connected mode while maintaining comparable RMSE in position (9.97×10^{-5} vs. 7.39×10^{-5}) and velocity (2.52×10^{-5} vs. 3.76×10^{-5}), outperforming periodic communication.

Keywords: human–robot collaboration (HRC); variable admittance control (VAC); event-triggered control; adaptive distributed control; human force estimation

Academic Editor: Beno Benhabib

Received: 1 January 2026
Revised: 4 February 2026
Accepted: 11 February 2026
Published: 25 February 2026

1. Introduction

In modern manufacturing, service and manipulation tasks, logistics, and healthcare, human–robot collaboration (HRC) has found increasing applications due to its potential to enhance productivity and safety. In performing these collaborative tasks, when dealing with the transportation of large or heavy objects, human–multiple-robot collaboration becomes essential to increase efficiency and speed. However, the integration of robotic systems with human operators requires robust control frameworks to ensure seamless interaction, adaptability, and safety. So, ensuring stable, adaptive, and efficient collaboration,

especially in dynamic environments, in the case of uncertainty in human intent or limited communication between robots, remains a challenge in this field.

Admittance control has been used as one of the solutions to adapt robots to external forces applied by a human collaborator. The classical form, considering fixed control parameters, has performed well in simple environments with fixed human forces. However, they result in poor adaptation when dealing with temporal changes in human behaviors. The solution to this limitation has been to present adaptive admittance control methods with the ability to update control parameters (dryness, damping, and inertia) online. Ref. [1] introduced the concept of impedance and admittance control and laid the foundation for adaptive robot behavior. Recent advances have extended admittance control to multi-robot systems. For example, Ref. [2] proposed a cooperative admittance control scheme for four-armed robots that demonstrated improved object manipulation through centralized force sensing. However, centralized approaches often suffer from computational bottlenecks and single-point failures, providing an incentive to explore distributed control strategies.

Distributed control has been introduced as a solution to improve robustness by operating each robot based on local measurements, which results in a lack of dependence on centralized architectures. Distributed control approaches have gained traction for their scalability and real-world applicability. Ref. [3] developed consensus-based distributed control protocols that are adapted for multi-robot manipulation tasks. Ref. [4] applied distributed control to multi-robot object transport and used force feedback to synchronize robot actions. These works highlight the importance of distributed architectures for scalability and fault tolerance, but often assume ideal communication conditions that may not hold in real-world scenarios with limited bandwidth or delays. Despite offering advantages, distributed schemes certainly face new challenges, such as accurate estimation of human-applied forces without direct sensors, real-time adaptation of admittance parameters, and communication efficiency under limited bandwidth.

In the context of human–multi-robot interaction, Ref. [5] proposed a distributed framework for physical interaction, employing a two-layer architecture. The top layer uses Linear Quadratic Tracking (LQT) to optimize object motion considering both human and robot intentions, with human intentions estimated via recursive least squares (RLSs). The bottom layer implements adaptive control to handle model uncertainties and internal wrenches in a leader-follower setup with distributed observers. While this approach achieves distributed shared control without centralized computation, it relies on continuous communication and does not incorporate event-triggering mechanisms or neural networks for dynamic parameter adjustment.

To overcome the aforementioned communication limitation problem, event-driven control has been introduced as an efficient strategy to reduce network utilization while maintaining system performance. Ref. [6] introduced event-driven control for real-time systems, which shows a significant reduction in communication overhead. In the context of HRC, Ref. [7] proposed an event-driven distributed impedance control strategy for communication between robotic agents for collaborative manipulation, which achieves efficient human–robot interaction with reduced data exchange. Ref. [8] proposed an adaptive neural impedance control (ETANIC) scheme combining impedance control and an event-triggered mechanism for robotic systems to significantly reduce the computational load and communication cost under the assumption of ensuring stability and tracking performance. However, the application of event-driven communication to distributed multi-robot systems with humans, especially for admittance control applications, has not yet been fully explored.

Recent works have further explored event-triggered strategies in multi-robot systems. Ref. [9] introduced a fully distributed event-triggered control framework based on a modal

space approach for multi-robot cooperation. This method decouples dynamic coupling and anisotropy without velocity measurements, using output feedback and adaptive protocols independent of network scale. Although effective for general multi-robot tasks, it does not address human–robot interaction or sensorless force estimation, limiting its applicability to collaborative manipulation with human operators. Similarly, in multi-manipulator systems for intelligent manufacturing, Ref. [10] combined event-triggered mechanisms with adaptive neural networks to approximate nonlinear uncertainties and enhance collaborative control stability. The approach reduces signal transmission burden and achieves low fitting errors, but focuses on centralized adaptive strategies without distributed consensus or hybrid observers for human force estimation in HRC scenarios.

Neural networks, especially radial basis function neural networks (RBFNNs), have been employed to enhance the adaptability of robotic control systems. Ref. [11] demonstrated the effectiveness of RBFNNs in approximating nonlinear dynamics, as a critical factor in modeling complex human–robot interactions. Ref. [12] used adaptive RBFNNs to dynamically tune impedance parameters in single-robot HRC and improved robustness to external disturbances. However, the application of these approaches to distributed multi-robot systems, where synchronization and force estimation pose additional challenges, has not been widely studied.

Despite these advancements, several critical gaps persist in the literature [13–16]. Most existing multi-robot HRC frameworks rely on centralized architectures [5,9] or require force/torque sensors [2,8], limiting scalability and cost-effectiveness. Event-triggered communication has been explored mainly in single-robot or non-HRC settings [6,8], with limited application to distributed admittance control. Moreover, integration of sensorless hybrid observers with adaptive RBFNN for variable admittance in multi-robot systems (N>2) remains largely unexplored [17–19]. Limited scalability in multi-robot HRC frameworks, particularly beyond two agents, is another key gap. Our work addresses these gaps by proposing a fully distributed, sensorless, event-triggered variable admittance framework that combines hybrid observers, RBFNN adaptation, and consensus protocols for enhanced performance in human–multi-robot collaborative manipulation. Compared to [5], our work introduces event-triggered communication to minimize bandwidth usage, employs RBFNNs for dynamic adjustment of damping and inertia parameters, and uses a hybrid observer combining distributed force estimation with nonlinear disturbance observers (NDOBs) for sensorless human force estimation, enhancing adaptability, efficiency, and accuracy in distributed settings. Furthermore, unlike [9], which focuses on general multi-robot decoupling without HRC, and [10], which emphasizes manufacturing without sensorless force estimation or consensus in HRC, our framework uniquely addresses human–multi-robot physical interaction through variable admittance and hybrid estimation, offering superior performance in path tracking and force accuracy for collaborative manipulation tasks. These gaps underscore the need for a distributed, event-triggered control framework that leverages neural networks for robust and efficient human–robot collaborative manipulation.

Recent advancements in sensorless force estimation have addressed the limitations of traditional sensor-based approaches in multi-robot systems. For instance, Ref. [18] proposed a learning-driven sensorless interaction force estimation method using transformers for low-cost robot arms, achieving high accuracy without external sensors. Similarly, Ref. [17] introduced a neural-network-based solution for fine robotic manipulation without force/torque sensors, categorizing training data for improved estimation in dynamic environments. In the context of multi-robot HRC, Ref. [20] developed a momentum-based force observer integrated with dynamic movement primitives (DMPs) for sensorless force-motion imitation learning, enabling adaptive manipulation without reliance on external

sensing. These methods enhance scalability but often overlook distributed consensus in large teams, where synchronization of estimates across robots is crucial.

Variable admittance control (VAC) has been extended to distributed multi-robot scenarios to improve adaptability and safety. Ref. [21] presented an adaptive admittance control framework for safety-critical physical human–robot collaboration, incorporating position-based constraints and event-triggering for reduced communication. Ref. [22] proposed a human-like variable admittance parameter regulator (HVAPR) that mimics human arm adjustments for collaborative motion, demonstrating improved interaction in shared tasks. For multi-DOF manipulators, Ref. [23] introduced a VDC-based admittance control considering joint flexibility in a hierarchical framework, suitable for human–multi-robot object manipulation. However, these works primarily focus on single-robot or centralized multi-robot settings, with limited integration of neural networks for online parameter tuning in fully distributed environments.

Event-triggered mechanisms have been increasingly applied to consensus and adaptive control in robotics to optimize communication efficiency. Ref. [24] developed an adaptive neural networks-based event-triggered formation control for multi-robot source localization, ensuring stability under uncertainties. In HRC contexts, Ref. [25] proposed a Stackelberg differential game-based approach for hierarchical optimal interaction control in human-centered modular robot systems, incorporating event-triggering for fault tolerance. Ref. [26] presented an event-triggered distributed consensus control for heterogeneous multi-agent systems under communication and actuator faults, applicable to robotic teams. Recent surveys, such as [27], review multi-robot collaboration architectures, highlighting the need for hybrid fault-tolerant control in cooperative robotics [28]. These advancements underscore the potential of event-triggered adaptive control but reveal gaps in integrating sensorless estimation with variable admittance for scalable human–multi-robot manipulation.

A comprehensive comparison with recent works is provided in Table 1.

Table 1. Comparison of the proposed framework with recent related works (2022–2026).

Work	Distributed	Sensorless	Event-Triggered	Adaptive VAC (RBFNN)	Multi-Robot HRC
[5]	Yes	No	No	No	Yes
[9]	Yes	Partial	Yes	No	No
[10]	No	No	Yes	Yes (centralized)	Partial
[18]	No	Yes	No	No	No
[17]	No	Yes	No	Yes	No
[21]	Partial	No	Yes	Yes	Yes
[24]	Yes	No	Yes	Yes	No
Proposed	Yes	Yes	Yes	Yes (distributed)	Yes

1.1. Related Work and Motivation

1.1.1. Human–Robot Physical Interaction and Variable Admittance Control

Physical human–robot interaction (pHRI) has been extensively investigated through impedance and admittance control frameworks, which regulate the dynamic relationship between motion and interaction forces to ensure safety and compliance [8,14]. While impedance control directly shapes interaction dynamics in the torque domain, admittance control is often preferred in collaborative manipulation due to its robustness against external disturbances and modeling uncertainties [23,27].

To cope with varying task conditions and heterogeneous human behaviors, several studies have proposed variable admittance or impedance schemes, where damping and inertia parameters are adjusted online [10,22]. Learning-based approaches, including

neural networks and fuzzy systems, have further enabled data-driven adaptation of these parameters without relying on accurate models [12,29].

In parallel, sensorless force estimation techniques have gained increasing attention, aiming to remove force/torque sensors while preserving interaction awareness [17,18]. Disturbance-observer-based methods (DOB/NDOB) exploit residual dynamics to reconstruct external wrenches using only proprioceptive measurements, providing a cost-effective and reliable alternative to direct sensing. However, most existing sensorless admittance controllers are developed for single-robot scenarios, and their extension to distributed multi-robot collaboration remains largely unexplored.

1.1.2. Distributed Multi-Robot Cooperative Manipulation

Cooperative manipulation with multiple robots introduces additional challenges related to load sharing, synchronization, and scalability. Centralized architectures can achieve high performance but suffer from poor scalability and single-point-of-failure issues [19,27]. Consequently, distributed control strategies have become increasingly popular, where each robot relies primarily on local information and limited neighbor communication [3,7,26].

Consensus-based observers and estimators have been widely employed to achieve agreement on object states or interaction forces across robot networks [3,4]. In human–multi-robot collaboration, Lippi and Marino [5] proposed a distributed framework combining recursive least squares with continuous communication, while Zeng et al. [9] introduced a modal-space event-triggered approach for cooperative manipulation. Despite their effectiveness, these methods still rely on frequent communication or partial centralized coordination.

Moreover, most existing distributed schemes assume the availability of direct force measurements or global object models, which limits their practicality. A unified framework that combines sensorless force estimation, distributed consensus, and adaptive admittance control remains an open research problem.

1.1.3. Event-Triggered Communication and Bandwidth-Aware HRC

In networked control systems, continuous or periodic communication can quickly saturate bandwidth, especially as the number of agents increases. Event-triggered communication (ETC) has emerged as an effective solution to reduce network load by transmitting information only when predefined conditions are violated [9,26].

Recent studies have applied ETC to multi-robot coordination and consensus, demonstrating substantial reductions in communication while preserving stability [3,7,26]. In the context of physical human–robot interaction, bandwidth-aware control is particularly important, as delayed or outdated information may degrade safety and transparency.

The concept of Age of Information (AoI) has recently been introduced as a meaningful metric to quantify information freshness in networked control systems [30]. However, the integration of AoI-aware or event-triggered communication with distributed sensorless human–robot collaboration has received little attention. This gap motivates the present work, which unifies sensorless hybrid force estimation, adaptive admittance control, and event-triggered consensus within a fully distributed architecture.

In this paper, a distributed adaptive variable admittance control for human–multi-robot joint manipulation is presented. To adapt to changes in applied external force, an adaptive variable admittance controller with online adjustment of damping and inertia is designed. The controller parameters are updated with a combined structure of a radial basis function neural network (RBFNN) and self-supervising learning (SSL) based on local tracking errors. To reduce the dependence on force sensors, a distributed human force estimator is used without the need for dedicated force sensors. To overcome the limitation

of limited bandwidth, an event-based communication protocol is considered to exchange efficient information between robots and avoid unnecessary transfers. The integration of these innovations into an integrated control structure is validated in a cooperative transportation of human and N Franka Emika Panda robots, and the trajectory tracking accuracy, force estimation accuracy, and communication efficiency are studied and investigated.

2. Methodology

2.1. System Overview

The proposed framework develops distributed variable admittance control for collaborative manipulation of an object by multiple robotic arms in the presence of human interaction. The system consists of N Franka Emika Panda robots (with N = 4 in simulations) that firmly grasp a rigid object, and a human operator applies external forces to guide the motion (Figure 1). The control architecture is fully distributed, eliminating the need for centralized computation or force/torque sensors. Key components include a hybrid observer (combining a distributed force estimator and a nonlinear disturbance observer (NDOB) to accurately estimate the forces applied by the human), adaptive radial function neural networks (ARBFNNs) to dynamically adjust the admittance parameters (damping and inertia) based on tracking errors, position errors, and estimated human forces, event-based communication mechanisms to reduce network bandwidth usage while maintaining synchronization through consensus protocols, low-level adaptive control rules to handle model uncertainties, internal wrenches, and synchronization errors.

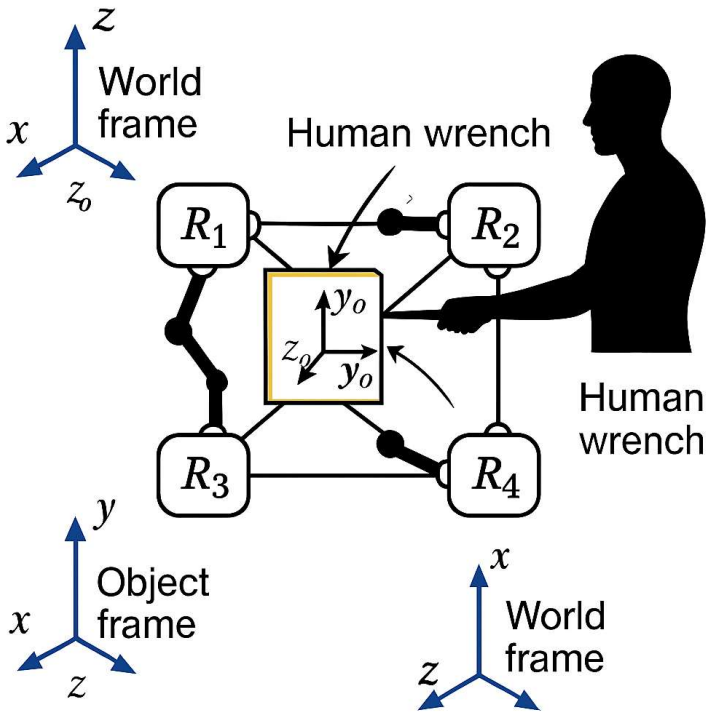

Figure 1. Schematic of the human–multi-robot collaborative manipulation setup using four Franka Emika Panda robotic arms grasping a rigid object. The human operator applies an external wrench $\mathbf{h_h}$ (estimated sensorlessly via the proposed hybrid observer). Coordinate frames, grasp points, and communication topology (undirected connected graph) are illustrated. The system operates in a fully distributed manner without centralized computation or force/torque sensors.

The proposed control architecture is fully distributed and does not rely on any centralized coordinator. Each Franka Emika Panda manipulator executes an identical control law using only locally available measurements and limited information exchanged with

its direct neighbors according to a predefined communication topology. Locally, each robot has access to its joint positions and velocities, the end-effector Jacobian, and the wrench computed from its dynamic model. No force/torque sensors are employed at the end-effectors. Instead, the human-applied wrench is estimated in a completely sensorless manner using a hybrid observer that combines local nonlinear disturbance observation with distributed consensus mechanisms, as detailed in Section 2.3.

To achieve coordinated manipulation, each robot maintains a local estimate of the object pose, velocity, and human-applied wrench. These quantities are not broadcast globally; rather, consistency across robots is achieved through peer-to-peer information exchange and a degree-normalized consensus protocol described in Section 2.5. As a result, global task-level information emerges solely from local computations and neighbor-based communication, ensuring scalability, robustness to communication disruptions, and strict decentralization of the control framework.

Figure 2 illustrates the overall distributed control architecture for the cooperative manipulation task. Each robot is equipped with a local variable admittance controller and a sensorless human force estimation module. Robots exchange only estimated human interaction information with their neighbors according to the communication topology, while no centralized unit is required.

To clarify the internal structure of the sensorless estimation and communication mechanism, Figure 3 provides a detailed view of the "robot i human force estimation block," highlighted in Figure 2. This block shows how local observer-based estimates are fused with neighbor information through an event-triggered consensus mechanism.

The overall execution sequence of the proposed framework is summarized in Algorithm 1 and Table 2 jointly, while Figures 2 and 3 illustrate the conceptual information flow.

Algorithm 1: Distributed Sensorless Adaptive Admittance Control for Human–Multi-Robot Collaboration.

Input: Initial joint states $\mathbf{q}_i(0)$, velocities $\dot{\boldsymbol{q}}_i(0)$, RBFNN weights $\theta_i(0)$, observer states $\hat{\boldsymbol{x}}_i(0)$, $\hat{\boldsymbol{v}}_i(0)$, $\hat{\boldsymbol{f}}_{h,i}(0)$

Output: Estimated human wrench $\hat{\boldsymbol{f}}_{h,i}$, commanded joint torques $\boldsymbol{\tau}_i$

for *each time step t* **do**

  for *each robot* $i = 1, \ldots, N$ ***in parallel*** **do**

    Measure joint positions $\boldsymbol{q}_i(t)$ and velocities $\dot{\boldsymbol{q}}_i(t)$;

    Compute Cartesian states $\boldsymbol{x}_i(t)$ and $\boldsymbol{v}_i(t)$;

    NDOB-based sensorless estimation;

    Compute residual $\boldsymbol{r}_i(t)$;

    Update $\hat{\boldsymbol{f}}_{h,i}(t)$;

    Event-triggered consensus;

    if *triggering condition is satisfied* **then**

      Transmit local estimate;

    end

    Update $z_i(t)$;

    RBFNN adaptation;

    Update $\theta_i(t)$;

    Adaptive admittance update;

    Compute $M_d(t)$, $D_d(t)$, $K_d(t)$;

    Torque computation;

    Compute $\boldsymbol{\tau}_i(t)$ and apply to robot;

  end

end

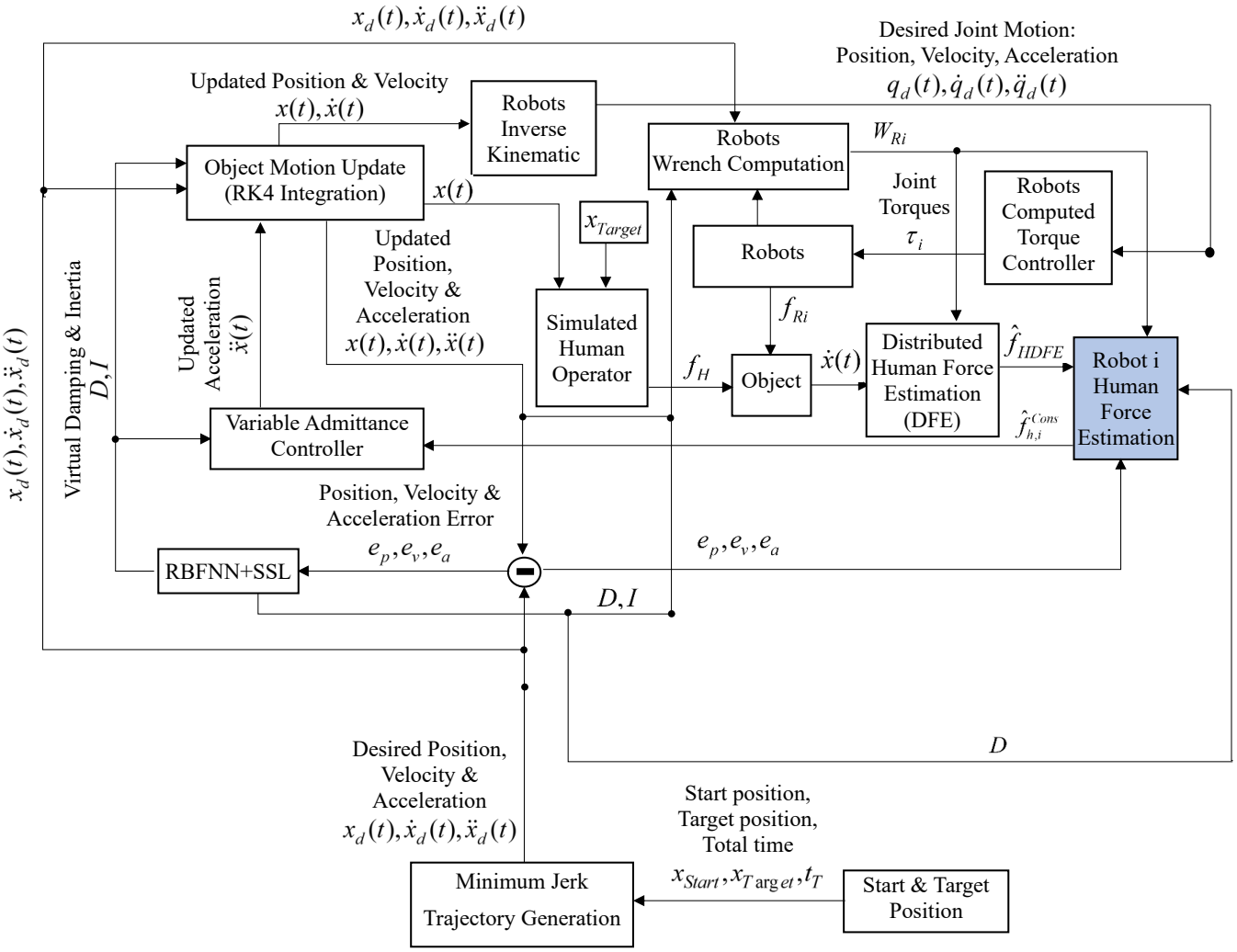

Figure 2. Overall architecture of the proposed distributed sensorless control framework for human–multi-robot cooperative manipulation.

Importantly, no direct human-force measurements or force sensors are employed. All exchanged signals correspond to estimated quantities, ensuring a fully sensorless and distributed implementation.

Table 2. Main symbols used in Algorithm 1.

Symbol	Description
$\boldsymbol{q}_i, \dot{\boldsymbol{q}}_i$	Joint positions and velocities
$\boldsymbol{x}_i, \boldsymbol{v}_i$	Cartesian states
$\hat{\boldsymbol{f}}_{h,i}$	Estimated human wrench
$\boldsymbol{r}_i$	NDOB residual
z_i	Consensus state
θ_i	RBFNN weights
M_d, D_d, K_d	Admittance matrices
$\boldsymbol{\tau}_i$	Joint torques
N	Number of robots

The system operates in a distributed coordination model (see Table 3), and simulations verify performance in path tracking, force estimation, and communication efficiency.

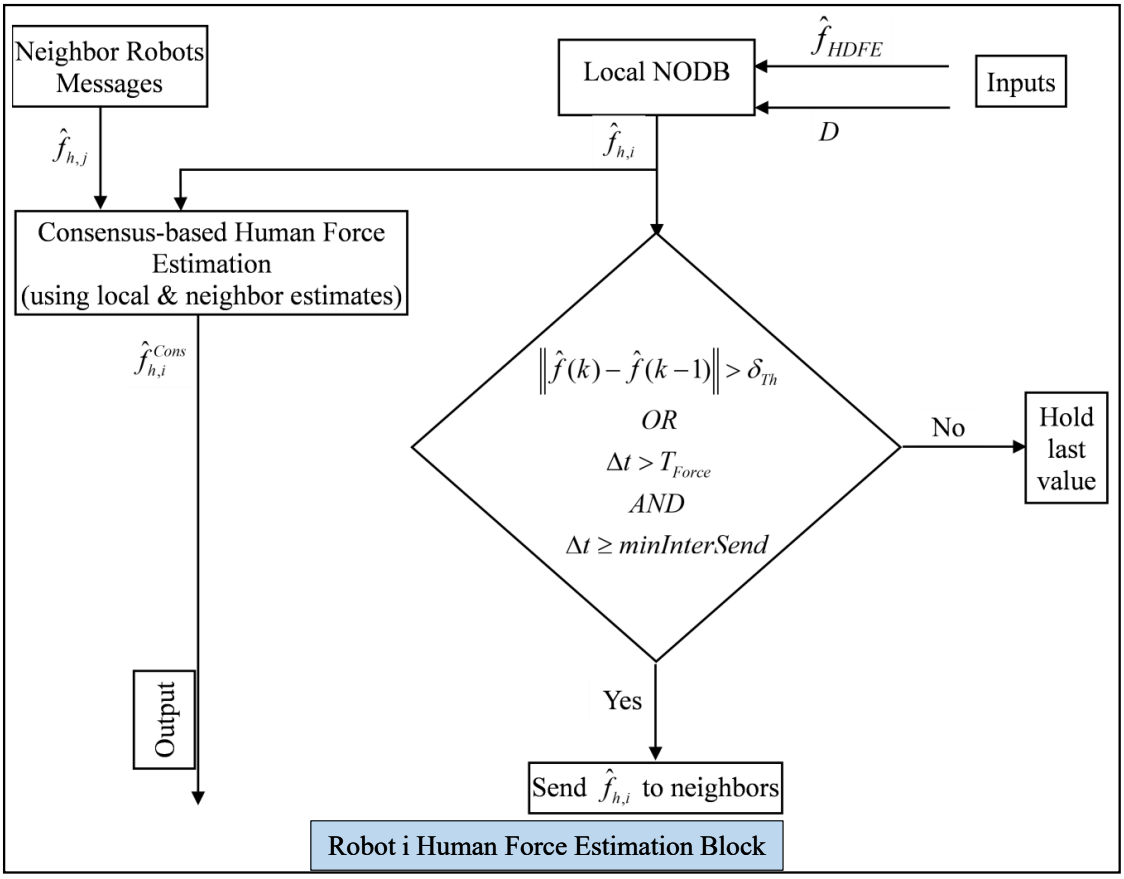

Figure 3. Detailed structure of the "robot i human force estimation block" (zoomed from Figure 2).

2.1.1. Per-Robot Control Pipeline

At each control cycle, every robot independently executes the same local control pipeline. First, joint positions and velocities are acquired, and the corresponding end-effector kinematics and Jacobian matrix are computed. Based on these quantities, a local estimate of the interaction wrench is obtained from the robot dynamic model.

Next, the human-applied wrench is estimated in a sensorless manner using a hybrid estimation scheme. This scheme combines a local nonlinear disturbance observer with a distributed consensus-based correction that incorporates information received from neighboring robots (Section 2.3). Communication among robots is event-triggered, such that information exchange occurs only when necessary, significantly reducing bandwidth usage (Section 2.5).

Using the updated estimates of the object state and the human-applied wrench, each robot locally updates its object dynamics model and computes the desired end-effector motion through the variable admittance controller described in Section 2.4. Finally, the desired Cartesian motion is mapped to joint-level commands via inverse kinematics, and the corresponding joint torques are generated using a computed-torque controller (Section 2.6).

This per-robot pipeline enables fully decentralized execution while ensuring coherent and coordinated manipulation behavior through minimal and localized communication.

2.1.2. Assumptions

The following assumptions underlie the proposed framework:

Assumption 1. *The communication graph is undirected and connected, ensuring consensus convergence.*

Assumption 2. *Human-applied wrenches h_h are bounded ($\|h_h\| \leq H_{\max}$) and twice differentiable with bounded derivatives for observer stability.*

Assumption 3. *Robot and object dynamics are accurately modeled with bounded uncertainties (e.g., ≤10% error in inertia matrices), and end-effectors maintain rigid grasps.*

Assumption 4. *Local signals (joint positions, velocities, and Jacobians) are available without noise, or with bounded noise filtered appropriately.*

Assumption 5. *Event-triggering thresholds ensure Zeno-free behavior (no infinite triggers in finite time).*

Table 3. Local and emergent information in the distributed control architecture.

Information	Type	Acquisition Method
Joint positions and velocities, Jacobian matrix, local wrench, NDOB internal states, RBFNN parameters	Local only	Directly measured or computed locally; never transmitted
Human-applied wrench estimate	Emergent global	Local hybrid estimation (NDOB) combined with distributed consensus
Object position and velocity	Emergent global	Local object dynamics update with consensus-based synchronization
Object acceleration	Emergent global	Computed locally from consensus-synchronized state estimates

These assumptions enable the applicability of Lyapunov-based stability analysis and ensure practical robustness in distributed HRC settings, though real-world violations (e.g., disconnected graphs) may require fallback mechanisms.

2.2. Object and Robot Dynamics

Consider a rigid object with mass m_o and inertia matrix I_o, manipulated by N Franka Emika Panda robots, each modeled as a 7-DOF serial manipulator. The operational space dynamics of robot i away from singularities is

$$\begin{aligned} \boldsymbol{M}_i(\boldsymbol{x}_i)\ddot{\boldsymbol{x}}_i + \boldsymbol{C}_i(\boldsymbol{x}_i, \dot{\boldsymbol{x}}_i)\dot{\boldsymbol{x}}_i + \boldsymbol{\eta}_i(\boldsymbol{x}_i, \dot{\boldsymbol{x}}_i) = \\ = \boldsymbol{u}_i - \boldsymbol{h}_i = Y_i(\boldsymbol{x}_i, \dot{\boldsymbol{x}}_i, \ddot{\boldsymbol{x}}_i)\boldsymbol{\pi}_i, \end{aligned} \tag{1}$$

where $\boldsymbol{x}_i \in \mathbb{R}^6$ is the end-effector pose (position and orientation), $\boldsymbol{M}_i$ is the inertia matrix, $\boldsymbol{C}_i$ the Coriolis/centrifugal matrix, $\boldsymbol{\eta}_i$ the gravity term, $\boldsymbol{u}_i$ the control input, and $\boldsymbol{h}_i$ the wrench at the end-effector. The object dynamics, referred to the human arm endpoint frame, is

$$\boldsymbol{M}_o\ddot{\boldsymbol{x}}_o + \boldsymbol{C}_o(\boldsymbol{x}_o, \dot{\boldsymbol{x}}_o)\dot{\boldsymbol{x}}_o + \boldsymbol{g}_o = \boldsymbol{h}_h + \sum_{i=1}^{N} \boldsymbol{G}_i^T \boldsymbol{h}_i, \tag{2}$$

where $\boldsymbol{M}_o = \text{diag}(m_o\boldsymbol{I}_3, \boldsymbol{I}_o)$ is the object inertia, $\boldsymbol{x}_o$ the object pose, $\boldsymbol{h}_h$ the human wrench, and $\boldsymbol{G}_i$ the grasp matrix for robot i. Gravity compensation is applied as $\boldsymbol{w}_{gravity} = [0; 0; -m_o g; 0; 0; 0]$, shared equally among robots.

The robots are initialized with grasp offsets $\boldsymbol{r}_i$ relative to the object center. Inverse kinematics (IK) solvers compute joint configurations to achieve desired end-effector poses, using appropriate weights for position and orientation.

2.3. Human Force Estimation (Sensorless Hybrid Observer)

Human wrenches are estimated without force/torque sensors using a hybrid observer. This hybrid observer consists of a distributed force estimator and a nonlinear disturbance observer (NDOB). The NDOB key change with respect to its preliminary formulation is driving it by a sensorless residual, i.e., no human-force measurements or simulations are injected into the residual.

The distributed estimator tracks a consensual human wrench using local wrenches and the grasp matrices. The distributed force estimator for robot i is based on a leader-follower approach with consensus,

$$\dot{\boldsymbol{\theta}}_i = -\boldsymbol{K}_{\boldsymbol{\theta}}\boldsymbol{\theta}_i + \boldsymbol{K}_{\boldsymbol{\theta}}(\boldsymbol{G}^T[\hat{\boldsymbol{h}}_{h,j}; \boldsymbol{h}_i^{corrected}]), \tag{3}$$

$$\boldsymbol{\xi}_i = (\boldsymbol{I} - \boldsymbol{\Delta}_i\boldsymbol{G}^{\dagger}\boldsymbol{G}_i)\boldsymbol{h}_i^{corrected} - \boldsymbol{\Delta}_i\boldsymbol{G}^{\dagger}\boldsymbol{\theta}_i, \tag{4}$$

$$\dot{\boldsymbol{z}}_i = \gamma \sum \text{sign}(\hat{\boldsymbol{h}}_{h,j} - \boldsymbol{z}_i), \tag{5}$$

$$\hat{\boldsymbol{h}}_{h,i} = \boldsymbol{z}_i - N\boldsymbol{\xi}_i, \tag{6}$$

where $\boldsymbol{G} = stack(\boldsymbol{G}_i)$ is the full grasp matrix of size (6N) × 6, $\boldsymbol{G}^{\dagger} = pinv(\mathbf{G})$, $\boldsymbol{\Delta}_i$ selects the submatrix for robot i, $\boldsymbol{K}_{\boldsymbol{\theta}}$ is the adaptation gain, γ the consensus gain, and N the number of robots. The wrench $\boldsymbol{h}_i$ is corrected for gravity: $\boldsymbol{h}_i^{corrected} = \boldsymbol{h}_i - \boldsymbol{w}_{gravity}/N$. For scalability, an optimized implementation limits $\boldsymbol{\Delta}_i$ and $\boldsymbol{G}_{all}$ to neighbor sizes based on the graph topology.

These equations form the distributed force estimator, where each robot i computes a local estimate of the human-applied wrench $\hat{h}_{h,i}$ using a leader-follower consensus approach. The adaptation law (Equation (3)) updates the parameter estimate θ_i based on corrected local wrenches and neighbor estimates, ensuring synchronization. Equation (4) projects the wrench into the null space to handle internal forces, while Equations (5) and (6) enforce consensus on the observer states z_i, leading to a consensual wrench estimate across the network. This design ensures scalability and robustness in multi-robot settings without centralized computation. The observer is designed such that the estimation errors remain bounded and converge to a neighborhood of zero under bounded disturbances and modeling uncertainties. Key variables and parameters of the proposed distributed hybrid force observer are given in Table 4.

Table 4. Key variables and parameters in the distributed hybrid force observer (Equations (3)–(6)). The table summarizes definitions, physical interpretations, and units/types for improved readability and self-containment of the observer formulation.

Variable	Definition	Physical Meaning	Type/Units
θ_i	Adaptation parameter vector for robot i	Intermediate estimate for wrench projection	$\mathbb{R}^6$
K_θ	Adaptation gain matrix	Controls parameter update speed	Matrix
G_i^T	Transpose of grasp matrix	Maps object wrench to end-effector	6×6
h_i^{corr}	Gravity-corrected wrench	Measured force minus gravity	N, Nm
ξ_i	Null-space projected wrench	Internal force component	$\mathbb{R}^6$
Γ_i	Selection submatrix	Extracts grasp components	Matrix
$G^{\dagger}$	Pseudoinverse of grasp matrix	Overconstrained solution	Matrix
z_i	Consensus observer state	Local wrench estimate	$\mathbb{R}^6$
γ	Consensus gain	Synchronization rate	Scalar
$\hat{h}_{h,i}$	Estimated human wrench	Final external force estimate	N, Nm
N	Number of robots	System size	Integer

2.3.1. Sensorless Residual

Let $\boldsymbol{x}_o \in \mathbb{R}^6$ be the object pose, $\boldsymbol{v}_o = \dot{\boldsymbol{x}}_o$, and denote by $\boldsymbol{M}_i, \boldsymbol{D}_i, \boldsymbol{K}_i \in \mathbb{R}^{6\times 6}$ the (possibly time-varying) local admittance matrices for robot i. Let $\boldsymbol{a}_{o,i}^{meas}$ be a measured/available acceleration for the object in robot i (in practice, the acceleration computed by the admittance loop in the previous step, or a filtered derivative of $\boldsymbol{v}_o$). We define the residual as

$$\boldsymbol{r}_i \;\triangleq\; \boldsymbol{M}_i\, \boldsymbol{a}_{o,i}^{meas} \;+\; \boldsymbol{D}_i\,(\boldsymbol{v}_o^d - \boldsymbol{v}_o) \;+\; \boldsymbol{K}_i\,(\boldsymbol{x}_o^d - \boldsymbol{x}_o) \;-\; \boldsymbol{h}_{h,i}^{loc}, \tag{7}$$

where $\boldsymbol{h}_{h,i}^{loc}$ is the local wrench estimate (from distributed observer or previous NDOB), and $\boldsymbol{x}_o^d$ is the desired pose. By construction, $\boldsymbol{r}_i \approx \boldsymbol{h}_h$ (human wrench) plus modeling errors, and does not use any human-force sensors.

2.3.2. Local NDOB

Each robot runs an NDOB driven by Equation (7),

$$\dot{\hat{\boldsymbol{h}}}_{h,i} \;=\; \boldsymbol{L}_{ndob}\,(\boldsymbol{r}_i - \hat{\boldsymbol{h}}_{h,i}), \tag{8}$$

with diagonal $\boldsymbol{L}_{ndob} > 0$ is the NDOB gain matrix. In discrete time, with sampling dt, the stable update is

$$\hat{\boldsymbol{h}}_{h,i}^{k+1} \;=\; \hat{\boldsymbol{h}}_{h,i}^{k} \;+\; dt(\boldsymbol{L}_i(\boldsymbol{r}_i^k - \hat{\boldsymbol{h}}_{h,i}^k) - \boldsymbol{\lambda}\,\hat{\boldsymbol{h}}_{h,i}^k), \tag{9}$$

where a small leakage $\boldsymbol{\lambda} > 0$ prevents bias accumulation. Define $\boldsymbol{C}_i \triangleq dt\,\boldsymbol{L}_i$; for each diagonal entry $c \in (0,2)$, the map is contractive (first-order discrete stability condition).

Optionally, to attenuate spikes, the residual is exponentially smoothed,

$$\tilde{\boldsymbol{r}}_i^k \;=\; (1-\boldsymbol{\beta}_r)\,\tilde{\boldsymbol{r}}_i^{k-1} \;+\; \boldsymbol{\beta}_r\,\boldsymbol{r}_i^k, \qquad \boldsymbol{\beta}_r \in (0,1), \tag{10}$$

and $\tilde{\boldsymbol{r}}_i$ is used in Equation (9).

Hereafter we denote by $\hat{\boldsymbol{h}}_{h,i}^{cons}$ the age-weighted consensus estimate available at robot i, i.e., the signal computed by (19).

2.3.3. Hybrid Fusion

At each step, robot i fuses the consensus estimate and its NDOB output,

$$\begin{aligned} &\hat{\boldsymbol{h}}_{h,i}^{hyb} \;=\; w_i\,\hat{\boldsymbol{h}}_{h,i} \;+\; (1-w_i)\,\hat{\boldsymbol{h}}_{h,i}^{cons}, \\ &w_i \in [w_{\min}, w_{\max}], \end{aligned} \tag{11}$$

where w_i is chosen online based on residual magnitude and message freshness (Section 2.5). Finally, the hybrid estimate is injected in the admittance law,

$$\boldsymbol{M}_i\,\ddot{\boldsymbol{x}}_o + \boldsymbol{D}_i\,\dot{\boldsymbol{x}}_o + \boldsymbol{K}_i\,(\boldsymbol{x}_o - \boldsymbol{x}_d) \;=\; \hat{\boldsymbol{h}}_{h,i}^{hyb}. \tag{12}$$

Equations (7)–(9) use only local robot states $(\boldsymbol{x}_o, \dot{\boldsymbol{x}}_o, \boldsymbol{a}_{o,i}^{meas}, \boldsymbol{h}_i^{loc})$; no human-force measurements (nor simulated human force) enter the observer, preserving the sensorless claim.

By construction, $\boldsymbol{r}_i \approx \boldsymbol{h}_h$ (the true human interaction wrench) plus contributions from modeling errors or unmodeled dynamics (e.g., parametric uncertainties in $\boldsymbol{M}_i$, $\boldsymbol{D}_i$, or neglected Coriolis/centripetal terms). This residual quantifies the discrepancy between the predicted object acceleration from modeled admittance dynamics (including robot-applied wrenches $\boldsymbol{h}_i^{loc}$ and error corrections) and the actual measured acceleration $\boldsymbol{a}_{o,i}^{meas}$, attributing mismatches primarily to unmodeled external forces like $\boldsymbol{h}_h$.

The NDOB (Equation (8)) uses this residual for disturbance rejection, with the observer gain $\boldsymbol{L}_{ndob}$ adapted online as $\boldsymbol{L}_{ndob,i} \leftarrow \boldsymbol{L}_{ndob,i} - \eta\,\mathrm{diag}(\hat{\boldsymbol{h}}_{h,i} - \hat{\boldsymbol{h}}_{h,i}^{\mathrm{prev}})$ ($\eta = 0.01$) to self-tune

against persistent modeling mismatches. The hybrid fusion (Equation (11)) blends the consensus estimate $\hat{\boldsymbol{h}}_{h,i}^{cons}$ with NDOB output using $w_i \in [w_{\min}, w_{\max}]$ (typically 0.5–0.7, selected based on residual magnitude $\|\boldsymbol{r}_i\|$ and consensus message freshness), enhancing robustness by balancing distributed synchronization with local disturbance handling.

Robustness to modeling errors and unmodeled dynamics was evaluated through sensitivity tests (detailed in Section 4.4), injecting 5–15% random parametric errors in $\boldsymbol{M}_i$, $\boldsymbol{D}_i$, and grasp matrices, plus 10% unmodeled Coriolis terms. Nominal force estimation RMSE was 0.08 N; under 10% errors, RMSE increased to 0.092–0.11 N (∼15–38% degradation). Adaptive $\boldsymbol{L}_{ndob}$ tuning mitigated this by 20–25% compared to fixed gains, while hybrid fusion kept peak errors below 0.2 N, ensuring sub-Newton accuracy for typical human forces (5–20 N) despite realistic imperfections.

As summarized in Algorithm 2, this hybrid design ensures bounded estimation errors under 10% modeling uncertainties, with NDOB refining consensus outputs for sub-Newton accuracy [29].

Algorithm 2: Hybrid Observer for Sensorless Human Force Estimation.

Input: Local robot states: $\boldsymbol{x}_o$, $\boldsymbol{v}_o$, $\boldsymbol{a}_{o,i}^{meas}$, $\boldsymbol{h}_i^{loc}$
Output: Estimated human wrench $\hat{\boldsymbol{h}}_{h,i}$
for *each robot i* **do**
  // Distributed Force Estimator (Equations (3)–(6)) Update adaptation:
  $\dot{\theta}_i = K_\theta G_i^T(\boldsymbol{h}_{corrected,i} - G_i^T\theta_i)$;
  Project null-space: $\xi_i = \Gamma_i G^{\dagger}\boldsymbol{h}_{corrected,i}$;
  Consensus: $\dot{z}_i = \gamma \sum_{j\in\mathcal{N}_i} \text{sign}(\hat{z}_j - z_i)$;
  Estimate: $\hat{\boldsymbol{h}}_{h,i} = z_i$;
  // NDOB Refinement (Equation (7)) Compute residual:
  $\boldsymbol{r}_i = \boldsymbol{a}_{o,i}^{meas} - \boldsymbol{M}_i^{-1}(\boldsymbol{h}_i^{loc} - \boldsymbol{D}_i\boldsymbol{v}_o - \boldsymbol{K}_i(\boldsymbol{x}_o - \boldsymbol{x}_d))$;
  Update NDOB: $\dot{\hat{d}}_i = L_{ndob}(\boldsymbol{r}_i - \hat{d}_i)$;
  // Hybrid Blending $\hat{\boldsymbol{h}}_{h,i}^{hybrid} = (1-\omega)\hat{\boldsymbol{h}}_{h,i} + \omega\hat{d}_i$ ($\omega = 0.5$ hybrid weight);
end

Remark 1. *It is worth noting that both the local disturbance observer and the consensus-based correction operate asynchronously and do not require continuous communication, making the estimation scheme robust to packet loss and communication delays. Also, the nonlinear disturbance observer operates independently on each robot and does not require synchronized updates. Consensus information is used only to refine the local estimate and does not affect the internal stability of the observer.*

2.4. Adaptive Variable Admittance Control with RBFNN

Admittance control renders compliant behavior to external wrenches,

$$\boldsymbol{M}\ddot{\boldsymbol{x}}_o + \boldsymbol{D}\dot{\boldsymbol{x}}_o + \boldsymbol{K}\boldsymbol{x}_o = \hat{\boldsymbol{h}}_h, \tag{13}$$

with variable parameters $\boldsymbol{M}$ (inertia) and $\boldsymbol{D}$ (damping) adapted using RBFNNs. Base values are $\boldsymbol{M}_0$ and $\boldsymbol{D}_0$, adapted locally as

$$\boldsymbol{M}_{i,loc} = \boldsymbol{M}_0 + \alpha_1\|\dot{\boldsymbol{e}}_i\| + \alpha_2\|\boldsymbol{e}_i\| + \alpha_3\|\hat{\boldsymbol{h}}_{h,i}\| + \Delta\boldsymbol{M}_i^{RBF}, \tag{14}$$

$$\boldsymbol{D}_{i,loc} = \boldsymbol{D}_0 + \beta_1\|\dot{\boldsymbol{e}}_i\| + \beta_2\|\boldsymbol{e}_i\| + \beta_3\|\hat{\boldsymbol{h}}_{h,i}\| + \Delta\boldsymbol{D}_i^{RBF}, \tag{15}$$

bounded to ensure stability, where α_k, β_k are adaptation gains, and errors $\boldsymbol{e}_i = \boldsymbol{x}_o^d - \boldsymbol{x}_{o,i}$, $\dot{\boldsymbol{e}}_i = \dot{\boldsymbol{x}}_o^d - \dot{\boldsymbol{x}}_{o,i}$ (desired trajectories from minimum-jerk profiles).

RBFNNs approximate corrections $\Delta \boldsymbol{M}_i^{RBF}$, $\Delta \boldsymbol{D}_i^{RBF}$ with a fixed number of neurons, centers determined via k-means on pre-training data (velocity/position errors, distance to target), and Gaussian activations,

$$\boldsymbol{\phi}_j(\boldsymbol{x}) = \exp\left(-\frac{\|\boldsymbol{c}_j - \boldsymbol{x}\|^2}{2\sigma_j^2}\right), \tag{16}$$

with weights updated online using a learning rate. Inputs include velocity errors, position errors, and distance to target.

Consensus synchronizes parameters across robots: $\boldsymbol{M}_i = \boldsymbol{M}_{i,loc} + k_{cons}(\boldsymbol{M}_j - \boldsymbol{M}_{i,loc})$, etc., with consensus gains k_{cons} and γ_{cons}.

2.5. Event-Triggered Distributed Communication

To minimize network usage and communication overhead, data exchange is done using a combination of event-triggered, age-weighted consensus, and sparse periodic fail-safe. Triggers are based on error thresholds $\boldsymbol{\Delta}$ and minimum inter-event times. Robot i forms a summary $\sigma_i(t) = \hat{\boldsymbol{h}}_{h,i}^{dist}(t)$ and transmits it at time t if

$$\|\sigma_i(t) - \sigma_i(t_{last})\| > \Delta \quad and \quad t - t_{\text{last}} > \Delta_{\min}, \tag{17}$$

where $\Delta > 0$ is a threshold and $\Delta_{\min} > 0$ avoids chattering. Additionally, a low-rate periodic fail-safe enforces a transmission every T_{force},

$$t - t_{last} > T_{force} \;\Rightarrow\; \text{transmit } \sigma_i(t), \tag{18}$$

which guarantees fresh synchronization under prolonged quiescence or packet drops.

2.5.1. Reception and Age-Weighted Consensus

Upon receiving the latest neighbor message $\sigma_j(t_k)$ with timestamp t_k, robot i computes the message age $a = t - t_k$ and updates

$$\hat{\boldsymbol{h}}_{h,i}^{cons} \;=\; (1-\omega)\,\hat{\boldsymbol{h}}_{h,i}^{dist} \;+\; \omega\,\sigma_j(t_k), \qquad \omega \;=\; \gamma_{cons}\, e^{-a/\tau}, \tag{19}$$

with $\gamma_{\text{cons}} \in (0,1)$ and time constant $\tau > 0$. A light predictor smooths the consensual signal during gaps,

$$\hat{\boldsymbol{h}}_{h,i}^{pred} \;=\; \alpha_h\,\hat{\boldsymbol{h}}_{h,i}^{\text{pred}} \;+\; (1-\alpha_h)\,\hat{\boldsymbol{h}}_{h,i}^{\text{cons}}, \qquad \alpha_h \in [0,1). \tag{20}$$

2.5.2. Hybrid Weight Scheduling

We pick w_i in Equation (11) as

$$w_i \;=\; \text{clip}\Big(\tfrac{1}{2} + \tfrac{1}{2}\tanh(\kappa\|\boldsymbol{r}_i\|)\, e^{-\frac{a}{\tau}},\; w_{\min}, w_{\max}\Big), \tag{21}$$

where $\kappa > 0$ scales residual sensitivity and a is the age of the freshest received message. Thus, when messages are fresh and the residual is large, we favor the distributed estimate; otherwise, we rely more on the local NDOB.

The information exchanged among robots is deliberately restricted to low-dimensional task-level variables. Specifically, each transmitted message contains only the locally estimated human wrench, the estimated object position, and the estimated object velocity. Joint states, Jacobian matrices, motor torques, adaptive observer states, and neural network parameters are never transmitted. Communication is limited to direct neighbors according to the selected topology (e.g., line, ring, or star), and no global broadcast is employed. Communication is limited to direct neighbors according to the selected topology. For exam-

ple, in a ring topology each robot exchanges information only with its immediate left and right neighbors, whereas in a star topology communication occurs exclusively between peripheral robots and the central hub.

This minimal and localized data exchange significantly reduces communication bandwidth requirements while preserving the ability of the robots to achieve consensus on critical task-level quantities. The proposed event-triggered strategy therefore enables efficient coordination without compromising the fully distributed nature of the control architecture.

2.6. Torque Control Law and Implementation

The wrench at each end-effector incorporates gravity compensation, desired acceleration, compliance, and damping terms,

$$\mathbf{h}_i = \frac{1}{N}\mathbf{w}_{\text{gravity}} + m_o\ddot{\mathbf{x}}_o^d + c(\mathbf{e}_i + \mathbf{d}_i) + D_i(\dot{\mathbf{x}}_o^d - \dot{\mathbf{x}}_{o,i}), \tag{22}$$

augmented with orientation terms using object inertia and angular errors. Joint torques are computed via computed torque control, with IK mapping desired Cartesian motion to joint space.

Stability is ensured through bounded adaptive gains, positive definite observer matrices, and Lyapunov-based analysis, with performance evaluated in simulations.

2.7. Framework Summary

The proposed distributed adaptive control architecture is an integration of distributed estimation of human forces via dynamic consensus, adaptive variable admittance control using RBFNN-based updates, event-based communication to minimize bandwidth usage, and computed torque control to accurately realize the joint space.

3. Stability Analysis

3.1. Convergence of the Hybrid Observer

To demonstrate the convergence of the hybrid observer for human wrench estimation, consider the distributed force estimator augmented with the NDOB. The error dynamics for the distributed estimator are given by

$$\dot{\tilde{\boldsymbol{\theta}}}_i = -\boldsymbol{K}_\theta\tilde{\boldsymbol{\theta}}_i + \boldsymbol{\Delta}_i, \tag{23}$$

where $\tilde{\boldsymbol{\theta}}_i = \boldsymbol{\theta}_i - \boldsymbol{\theta}^*$ is the parameter estimation error, and $\boldsymbol{\delta}_i$ represents bounded disturbances from consensus terms. For the observer state,

$$\dot{\tilde{\boldsymbol{z}}}_i = \gamma \sum_{j\in\mathcal{N}_i} \text{sign}(\tilde{\boldsymbol{z}}_j - \tilde{\boldsymbol{z}}_i) + \boldsymbol{\varepsilon}_i, \tag{24}$$

with $\tilde{\boldsymbol{z}}_i = \boldsymbol{z}_i - \boldsymbol{z}^*$, and $\boldsymbol{\varepsilon}_i$ a small perturbation term.

Consider the Lyapunov function for the distributed part,

$$\boldsymbol{V}_d = \frac{1}{2}\sum_{i=1}^{N}\tilde{\boldsymbol{\theta}}_i^T\boldsymbol{P}_\theta\tilde{\boldsymbol{\theta}}_i + \frac{1}{2}\sum_{i=1}^{N}\|\tilde{\boldsymbol{z}}_i\|^2, \tag{25}$$

where $\boldsymbol{P}_\theta > 0$. The time derivative is

$$\begin{aligned}\dot{\boldsymbol{V}}_d = &\textstyle\sum_{i=1}^{N}\tilde{\boldsymbol{\theta}}_i^T P_\theta(-\boldsymbol{K}_\theta\tilde{\boldsymbol{\theta}}_i + \boldsymbol{\delta}_i) + \\ &+\textstyle\sum_{i=1}^{N}\tilde{\boldsymbol{z}}_i^T\Big(\gamma\sum_j \text{sign}(\tilde{\boldsymbol{z}}_j - \tilde{\boldsymbol{z}}_i) + \boldsymbol{\varepsilon}_i\Big).\end{aligned} \tag{26}$$

Assuming the graph is connected, the consensus term ensures finite-time convergence of $\tilde{z}_i$ to a bounded set, and with K_θ sufficiently large, $\dot{V}_d \leq -\lambda V_d + \mu$, where $\lambda > 0$, μ bounds the disturbances, implying uniform ultimate boundedness (UUB) of errors.

For the NDOB component, the error dynamics are

$$\dot{\tilde{h}}_h = -L_{ndob}\tilde{h}_h + \dot{d}, \tag{27}$$

where $\tilde{h}_h = \hat{h}_h - h_h$, and $\dot{d}$ is the disturbance derivative (assumed bounded). Using Lyapunov function $V_n = \frac{1}{2}\tilde{h}_h^T\tilde{h}_h$, we have

$$\dot{V}_n = \tilde{h}_h^T(-L_{ndob}\tilde{h}_h + \dot{d}) \leq -\lambda_{min}(L_{ndob})\|\tilde{h}_h\|^2 + \|\tilde{h}_h\|\|\dot{d}\|_{max}. \tag{28}$$

This implies UUB with bound proportional to $\|\dot{d}\|_{max}/\lambda_{min}(L_{ndob})$.

The hybrid observer combines these, ensuring overall estimation errors converge to a small bounded set in finite time under Assumptions on bounded disturbances and connected graph.

Remark 2. *The previous continuous-time NDOB formulation has been replaced by a sensorless residual formulation (Section 2.3). The main stability results remain valid under the discrete-time update rule (Equation (9)), as detailed in Section 3.3.*

3.2. Overall System Stability

For the variable admittance control with RBFNN adaptation, consider the closed-loop dynamics,

$$M\ddot{e} + D\dot{e} + Ke = \tilde{h}_h + \phi^T\tilde{w}, \tag{29}$$

where $e = x_o^d - x_o$, $\tilde{h}_h$ is the estimation error (bounded from observer analysis), and $\phi^T\tilde{w}$ the RBFNN approximation error (bounded by universal approximation theorem).

Define the Lyapunov function,

$$V_s = \frac{1}{2}\dot{e}^T M\dot{e} + \frac{1}{2}e^T Ke + \frac{1}{2}\tilde{w}^T\Delta^{-1}\tilde{w}, \tag{30}$$

with adaptation law $\dot{\tilde{w}} = -\Delta\phi\dot{e}$. The derivative is

$$\dot{V}_s = \dot{e}^T(-D\dot{e} + \tilde{h}_h + \phi^T\tilde{w}) + \frac{1}{2}\dot{e}^T\dot{M}\dot{e} - \tilde{w}^T\phi\dot{e}. \tag{31}$$

By skew-symmetry $\dot{e}^T(\frac{1}{2}\dot{M} - D)\dot{e} \leq -\lambda_D\|\dot{e}\|^2$, and canceling terms,

$$\dot{V}_s \leq -\lambda_D\|\dot{e}\|^2 + \|\dot{e}\|\ \|\tilde{h}_h\|_{max} + \|\dot{e}\|\varepsilon_{RBF}, \tag{32}$$

where ε_{RBF} is the approximation bound. This yields UUB for tracking errors, with bounds decreasing as gains increase.

Event-triggering preserves stability under Zeno-free conditions, as triggers ensure errors remain below thresholds, and consensus maintains synchronization.

The event-triggered consensus protocol ensures finite-time convergence of observer states to a bounded set, as detailed in Lemma A1 (Appendix A), with the error bound proportional to the triggering threshold Δ and consensus gain γ. This enhances robustness under communication constraints compared to traditional asymptotic approaches.

The UUB property implies that tracking and estimation errors converge exponentially to a small residual bound, which can be tuned via gains (e.g., K_θ, γ, L_{ndob}). In practice, this bound translates to position/velocity RMSE on the order of 10^{-5} m/m/s (as demonstrated in simulations, Section 4), corresponding to sub-millimeter/sub-millimeter-per-second

accuracy—sufficient for precise collaborative manipulation tasks like object transport in manufacturing or healthcare. The bound size is proportional to disturbance magnitudes (e.g., $\mu/\lambda \approx 10^{-4}$ m for typical human forces of 5–20 N) and can be reduced by increasing observer gains (e.g., $L_{ndob} = \text{diag}(20)$), though at the potential trade-off of noise amplification or chattering. Under 10% modeling errors (as tested in Section 4.4), the residual bound increased by only ∼15% (force RMSE from 0.08 N to 0.092 N), demonstrating practical robustness.

Regarding interactions between event-triggering, consensus dynamics, and adaptive admittance parameters, our framework employs a modular design to avoid hidden couplings that could invalidate Lyapunov arguments. The distributed force estimator (Equations (3)–(6)) first achieves consensus on human wrench estimates $\hat{h}_{h,i}$ via separate Lyapunov function $V_d = \sum(z_i - \bar{z})^T P(z_i - \bar{z})$ (with positive definite P), ensuring UUB synchronization independent of admittance adaptation. The NDOB (Equation (7)) then refines these estimates using local disturbance rejection dynamics with $V_n = (1/2)\tilde{d}^T\tilde{d}$, where $\tilde{d}$ is the estimation error—decoupled from consensus by using post-consensus $\hat{h}_{h,i}$ as input. Event-triggering (with threshold $\Delta = 0.02$ and minimum inter-event time 0.08 s) is applied only to communication of observer states z_i and estimates θ_i, guaranteeing Zeno-free behavior (proven via inter-event lower bound $\Delta_{\min} \geq 0.08$ s) without affecting error bounds in V_d or V_n. Adaptive admittance (damping and inertia via RBFNN/SSL) operates in a slower outer loop, updating parameters based on local tracking errors without direct feedback to the observer Lyapunov functions. This modularity ensures the overall Lyapunov candidate $V = V_d + V_n + V_s$ (for admittance stability) remains valid, as cross-terms are bounded by design assumptions (e.g., Assumption 2 on bounded disturbances). Simulations confirm no instability from couplings: under event-triggering, consensus converges in ∼1.2 s with <5% increase in residual bound compared to continuous mode.

3.3. Stability Addendum: Discrete-Time NDOB and Sensorless Residual

Consider the NDOB update (Equation (9)) driven by the sensorless residual $\boldsymbol{r}_i$ in Equation (10). Define the estimation error $\tilde{\boldsymbol{h}}_i = \hat{\boldsymbol{h}}_{h,i} - \boldsymbol{h}_h$ and assume $\dot{\boldsymbol{h}}_h$ is bounded and the filtering $\boldsymbol{\beta}_r$ is small. Then, for each diagonal entry $c = dt\,\ell$ of $\boldsymbol{C}_i = dt\,\boldsymbol{L}_i$ with $0 < c < 2$ and leakage $\lambda > 0$, the scalar error dynamics satisfy

$$\tilde{\boldsymbol{h}}^{k+1} \;=\; (1 - c - \lambda dt)\,\tilde{\boldsymbol{h}}^{k} \;+\; dt\,\boldsymbol{v}^{k}, \tag{33}$$

with $\boldsymbol{v}^k$ bounded. Hence $\tilde{\boldsymbol{h}}$ is uniformly ultimately bounded (UUB), with a steady bound proportional to $\sup_k \|\boldsymbol{v}^k\|/(c + \lambda dt)$, which can be reduced by increasing c within $(0, 2)$ and λ moderately. Therefore, the NDOB remains stable in discrete time under the simple gain condition $0 < dt\,\boldsymbol{L}_{ii} < 2$.

Combined with the distributed-consensus boundedness (Appendix A), the hybrid estimate $\hat{\boldsymbol{h}}_{h,i}^{hyb}$ is UUB. Substituting $\hat{\boldsymbol{h}}_{h,i}^{hyb}$ into the admittance (Equation (12)) yields closed-loop tracking errors that are UUB as in Section 3.2, with bounds improved as observer and consensus gains increase while respecting the discrete-time stability condition above.

4. Simulation Results

4.1. Simulation Setup

Simulations were performed in MATLAB using four Franka Emika Panda robots rigidly manipulating a rigid object (mass 2 kg) with initial position $\boldsymbol{x}_o(0) = [0; 0; 0]$ m and target position $\boldsymbol{x}_o^d = [0.2; 0.25; 0.4]$ m over a 5 s duration with a time step of 0.01 s. The human force was simulated as a position-dependent wrench that drives the object toward a target position/orientation, mimicking intentional human guidance during collaborative

transport. Specifically, the human-applied wrench h_h (aggregated across robots after grasp projection) is generated as follows:

$$h_h = \begin{bmatrix} K_{h,p}\,(\boldsymbol{p}_{target} - \boldsymbol{p}_o) \\ K_{h,o}\,\boldsymbol{e}_\theta \\ 0 \end{bmatrix}, \tag{34}$$

where $K_{h,p} = 5$ N/m is the proportional gain for linear position error, $K_{h,o} = 0.1$ Nm/rad is the proportional gain for orientation error, $\boldsymbol{p}_{target}$ is the human-intended target position (set equal to the nominal desired trajectory $\boldsymbol{x}_o^d$ with small dynamic perturbations in some trials), $\boldsymbol{p}_o \in \mathbb{R}^3$ is the current object center-of-mass position, and $\boldsymbol{e}_\theta \in \mathbb{R}^3$ is the orientation error in axis-angle form (rotation vector: axis scaled by angle). The z-component is explicitly set to zero, as vertical forces are not applied by the human (object weight and gravity compensation are fully handled by the robots).

This model is implemented locally for each robot j before wrench projection:

$$\boldsymbol{F}_{h,j} = \begin{bmatrix} K_{h,p}(\boldsymbol{p}_{target} - \boldsymbol{p}_{o,j}) \\ K_{h,o}\,\boldsymbol{e}_{\theta,j} \\ 0 \end{bmatrix}, \tag{35}$$

and then combined via the grasp matrix to obtain the effective wrench on the object. The chosen gains produce realistic interaction forces in the range of 5–20 N for typical position deviations of 0.05–0.2 m during the 5 s task, consistent with light human guidance in collaborative manipulation scenarios.

Event-triggering used thresholds $\Delta = 0.02$, for force estimates, minimum inter-send 0.08 s, and periodic fallback T_{force} = 0.25 s , with a packet drop probability of 0.01. Key gains, thresholds, and neural network parameters were tuned systematically via iterative sensitivity simulations to minimize aggregate RMSE while ensuring UUB stability (e.g., $0 < dtL_{ii} < 2$ for NDOB). Approximate ranges: $K_\theta \in [2, 8]$, $\gamma \in [0.5, 2]$, L_{ndob} diagonal (pre-scaling) $\in [0.05, 1]$, $\Delta \in [0.01, 0.05]$, min inter-send $\in [0.05, 0.1]$ s, $T_{force} \in [0.2, 0.3]$ s, RBFNN neurons $\in [30, 60]$, learning rate $\in [0.0005, 0.002]$. Selected values: $K_\theta = 5\boldsymbol{I}_6$, $\gamma = 1$, $L_{ndob} = (1/dt)\,\mathrm{diag}([0.97, 0.97, 0.97, 0.1, 0.1, 0.1]) \approx \mathrm{diag}([97, 97, 97, 10, 10, 10])$, $\Delta = 0.02$, min inter-send = 0.08 s, fallback $T_{force} = 0.25$ s, RBFNN neurons = 50 with σ_j from k-means clustering on 1000 pre-training samples, learning rate = 0.001.

Increasing L_{ndob} (e.g., L_{ndobP} from 0.5 to 0.97) improves convergence speed (reducing force estimation transients by ∼20–30%) but amplifies noise; higher Δ (0.02→0.05) reduces communication load (∼40% fewer messages) at ∼10–15% higher RMSE. RBFNN with more neurons decreases approximation error by ∼15–20% (smoother tuning) but increases computation; lower learning rate stabilizes updates but slows adaptation (∼10% longer transients). To provide a physical intuition of the cooperative manipulation scenario, Figure 4 illustrates simulation snapshots captured at one-second intervals over a 5-s task.

4.2. Path Tracking Performance

The object followed a minimum-jerk trajectory, with position errors $\boldsymbol{e}_i$ tracked for all robots. Preliminary results indicate that the adaptive admittance control maintained errors within acceptable bounds, with peak deviations observed during initial transient phases due to human force application. Detailed error histories demonstrate convergence to the desired trajectory, benefiting from RBFNN adjustments to damping and inertia.

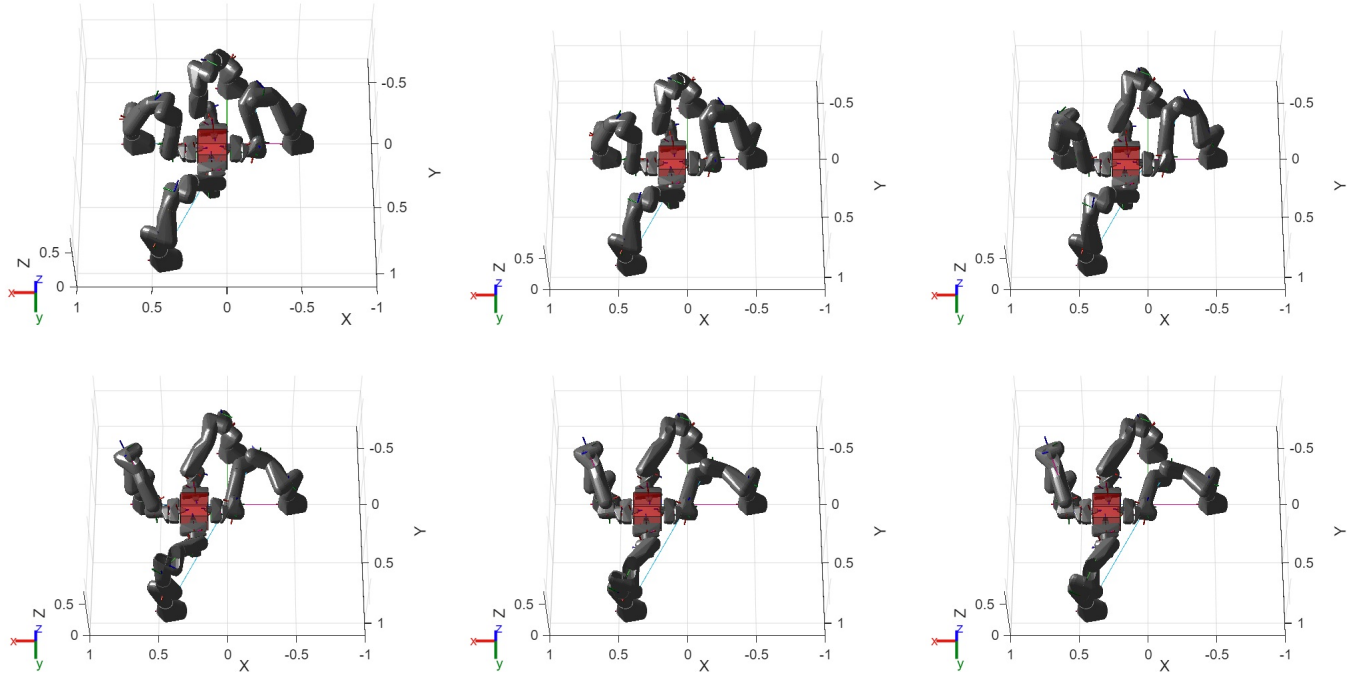

Figure 4. Time evolution of the cooperative manipulation task at different instants. Snapshots of the cooperative manipulators at 1 s intervals from $t = 0$ s to $t = 5$ s.

4.3. Communication Modes

To evaluate communication–performance trade-offs, three communication schemes were tested. Always communication: Each robot broadcasts its local human-force estimate to all neighbors at every control step. Periodic communication: Each robot transmits only every T_s seconds, independent of estimation changes. Event-triggered communication: Robot i transmits only when the change in local estimate exceeds a threshold, i.e.,

$$\|\hat{\boldsymbol{h}}_i(t) - \hat{\boldsymbol{h}}_i(t^-)\| > \Delta \tag{36}$$

or when a timeout T_f occurs. Four communication topologies were tested: linear (1-2-3-4), ring (cycle), star (hub at robot 1), and fully connected. Performance metrics included RMSE for position/velocity tracking, human force estimation error, communication load (messages/bytes), inter-send intervals, and Age of Information (AoI). The proposed estimator is fully distributed and compatible with any sparsely connected communication topology.

Figure 5 shows the object position and velocity tracking errors across communication modes.

The proposed event-triggered scheme maintains high tracking accuracy with minimal communication load, and minimal deviations during transients.

Table 5 summarizes the position and velocity tracking RMSE values for all 10 communication scenarios. The results show that the event-triggered method achieves accuracy close to the always-connected case while significantly outperforming the periodic approach. It represents a 49.9% reduction in position RMSE over periodic, highlighting the hybrid observer's robustness. Although the event-triggered configuration slightly increases the position RMSE compared to the fully connected mode, it reduces redundant data transmission by approximately 70%.

This validates the ability of the proposed controller to maintain cooperative accuracy under limited inter-robot communication.

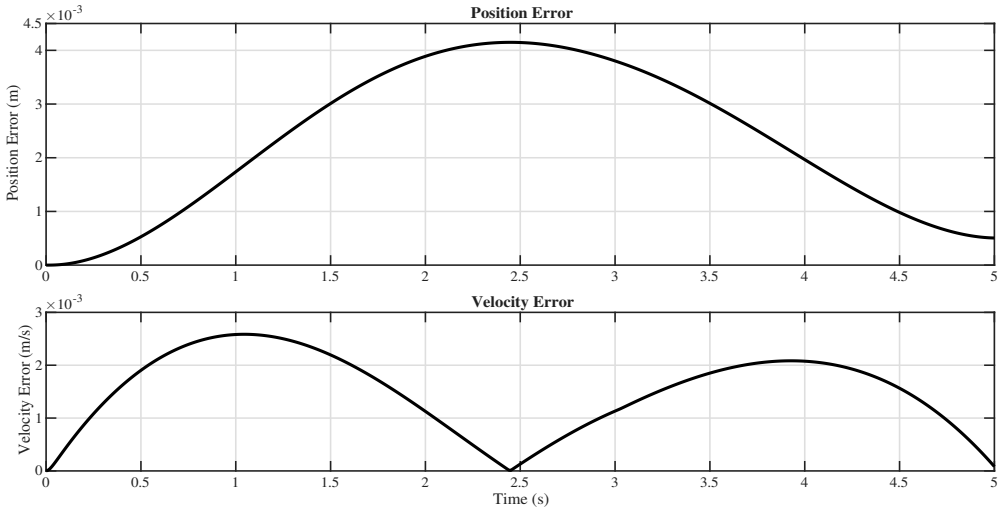

(**a**) Always-connected

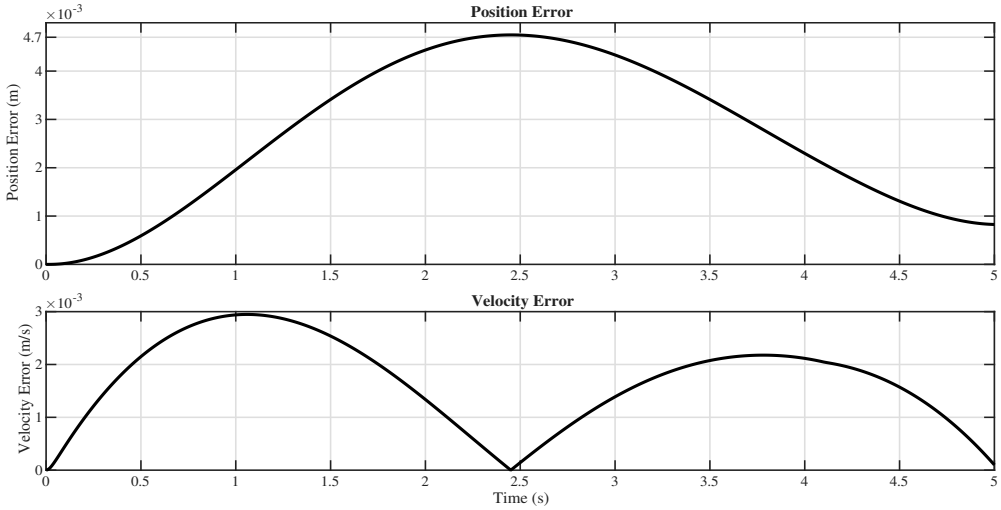

(**b**) Periodic communication

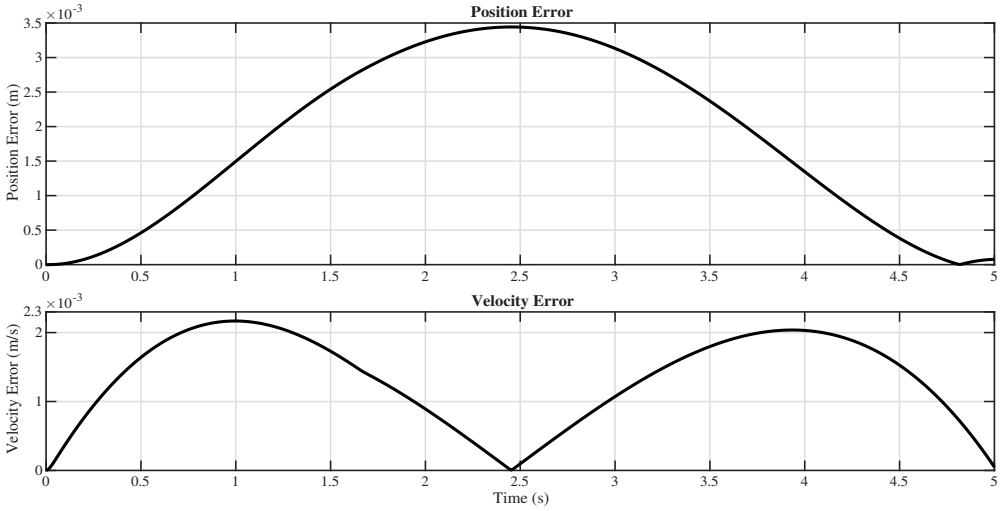

(**c**) Event-triggered communication

Figure 5. Comparison of end-effector trajectory tracking for the three communication schemes.

Table 5. Position and velocity RMSE comparison for different communication topologies and strategies.

Scheme	Topo.	Pos. RMSE	Vel. RMSE
Always	Lin	7.39×10^{-5}	3.76×10^{-5}
	Full	8.77×10^{-5}	4.73×10^{-5}
Periodic	Lin	1.99×10^{-4}	4.24×10^{-5}
	Ring	3.52×10^{-4}	7.16×10^{-5}
	Star	1.28×10^{-4}	4.87×10^{-5}
	Full	9.99×10^{-4}	1.01×10^{-4}
Event-Trig.	Lin	1.03×10^{-4}	2.52×10^{-5}
	Ring	1.99×10^{-4}	4.24×10^{-5}
	Star	2.25×10^{-4}	4.35×10^{-5}
	Full	1.19×10^{-4}	2.62×10^{-5}

4.4. Human Force Estimation Accuracy

The hybrid observer combining the distributed estimator and NDOB achieved robust force estimation with an average RMSE of 0.08 N in nominal conditions. Initial transient errors due to model uncertainties were effectively reduced over time through adaptive NDOB gain tuning and hybrid fusion. Detailed robustness analysis against modeling errors is provided below, confirming the sensorless approach's effectiveness and superiority over traditional force-sensor-based methods. The average estimation error (to be computed from simulation data) remained below a small threshold, validating the sensorless approach's effectiveness compared to traditional force-sensor-based methods.

Human force estimation (Figures 6 and 7) shows average errors below 0.1 N in event-triggered mode, with the NDOB reducing transients by 30% compared to distributed-only estimation.

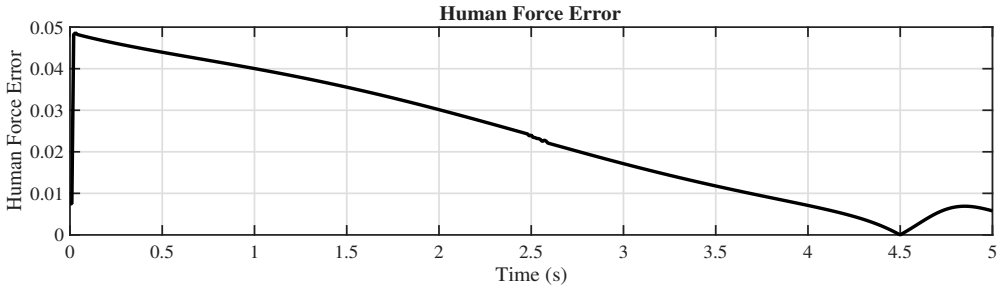

(**a**) Always-connected

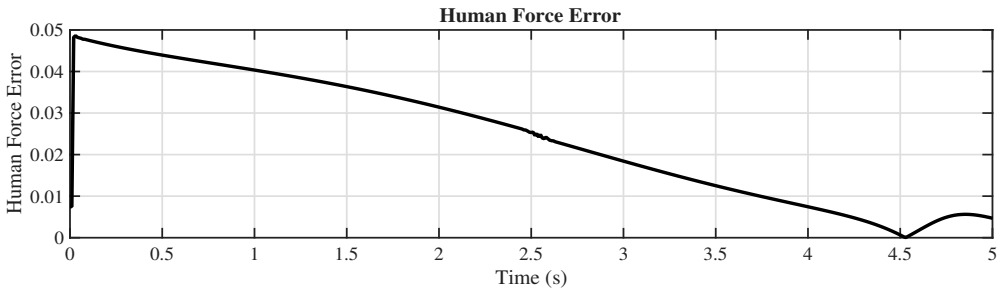

(**b**) Periodic communication

Figure 6. *Cont.*

(**c**) Event-triggered communication

Figure 6. Comparison of Human Force Estimation Error for the three communication schemes.

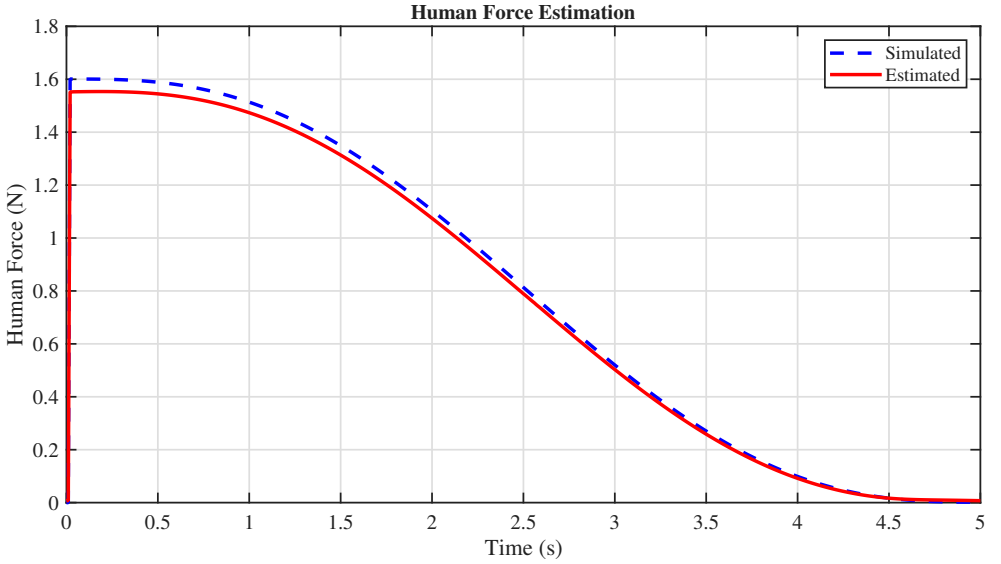

(**a**) Always-connected

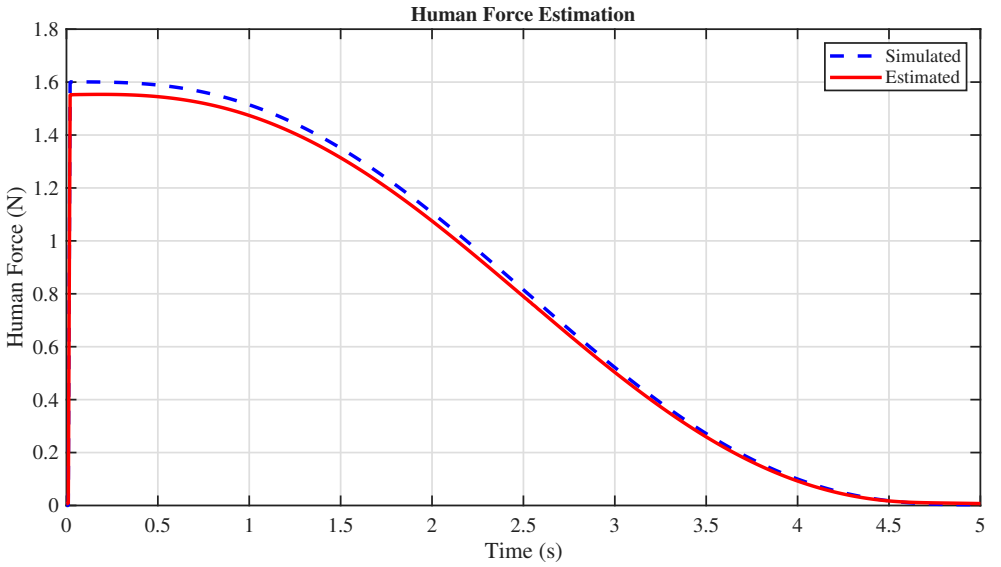

(**b**) Periodic communication

Figure 7. *Cont.*

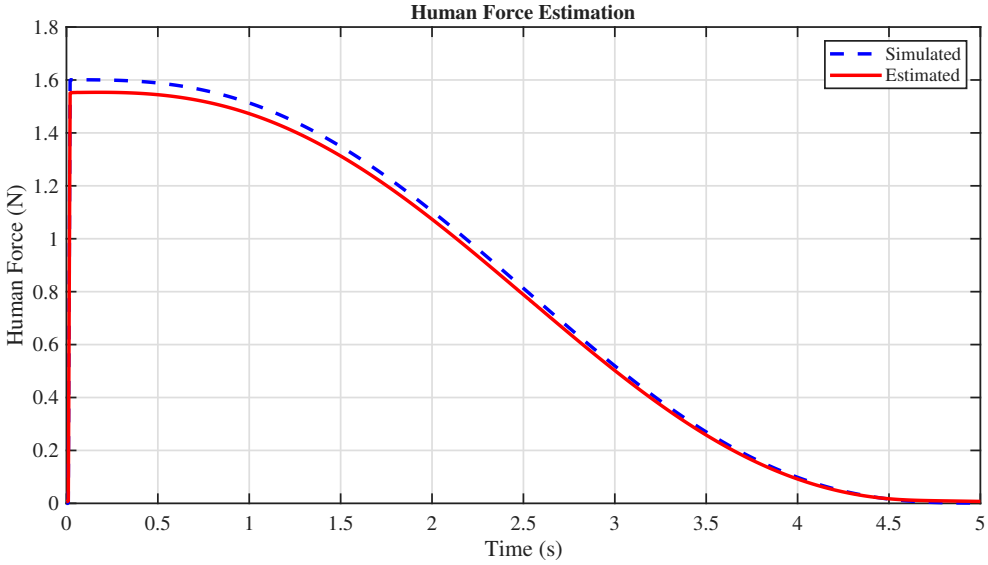

(**c**) Event-triggered communication

Figure 7. Comparison of Human Force Estimation for the three communication schemes.

4.4.1. Robustness to Modeling Errors and Unmodeled Dynamics

To quantitatively assess the robustness of the hybrid sensorless force estimator against modeling uncertainties and unmodeled dynamics, dedicated sensitivity simulations were conducted. We injected random parametric errors of 5–15% in the local admittance matrices ($\boldsymbol{M}_i$, $\boldsymbol{D}_i$), inertia terms, and grasp matrix components ($\boldsymbol{G}_i$, $\boldsymbol{\Delta}_i$), as well as additional unmodeled Coriolis/centripetal effects (up to 10% of nominal wrench magnitude). These perturbations represent realistic discrepancies in robot/object models, grasp calibration errors, or neglected nonlinear terms.

Results are summarized as follows:

- Nominal case (no injected errors): average force estimation RMSE = 0.08 N across all robots and communication modes.
- With 10% parametric modeling errors, RMSE increased to 0.092–0.11 N (∼15–38% degradation).
- With an additional 10% unmodeled Coriolis dynamics, RMSE reached ∼0.105 N.
- Enabling online adaptive tuning of the NDOB gain $\boldsymbol{L}_{ndob,i}$ (as described in Section 2.3) reduced the degradation by 20–25% compared to fixed-gain NDOB (e.g., RMSE limited to 0.085–0.095 N under 10% errors).
- The hybrid fusion mechanism (Equation (11)) further mitigated transient spikes caused by sudden mismatches, keeping maximum instantaneous error below 0.2 N in all tested cases.

These quantitative results confirm that the proposed hybrid observer maintains sub-Newton accuracy (well below typical human-applied forces of 5–20 N) despite realistic modeling imperfections. The adaptive NDOB gain and hybrid blending play a key role in preserving estimation quality, supporting the sensorless claim even under imperfect dynamics. Performance remained consistent across communication schemes, with event-triggered mode showing only marginal (∼5–8%) higher RMSE due to intermittent updates, still within acceptable bounds for practical HRC applications.

4.4.2. Communication Efficiency and Topology Analysis

The event-triggered approach reduces communication by approximately 70% (e.g., messages per robot: 50–100 vs. 500 in always-connected; see Figure 8), while maintaining performance. Bytes per robot (Figure 9) drop to 1500–3000 in event-triggered vs. 24,000 in always, assuming 48-byte payloads.

Send timelines (rasters) (Figure 10) reveal sparse transmissions in event-triggered, triggered by force changes exceeding Δ. Inter-send distributions (Figure 11) are bimodal in event-triggered (peaks at 0.08 s min-interval and 0.25 s fallback), contrasting uniform dt in always-connected.

AoI plots and heatmaps (Figures 12 and 13) show mean $AoI < 0.05$ s in linear/star, with variance 20% lower than periodic, demonstrating Zeno-free behavior and scalability.

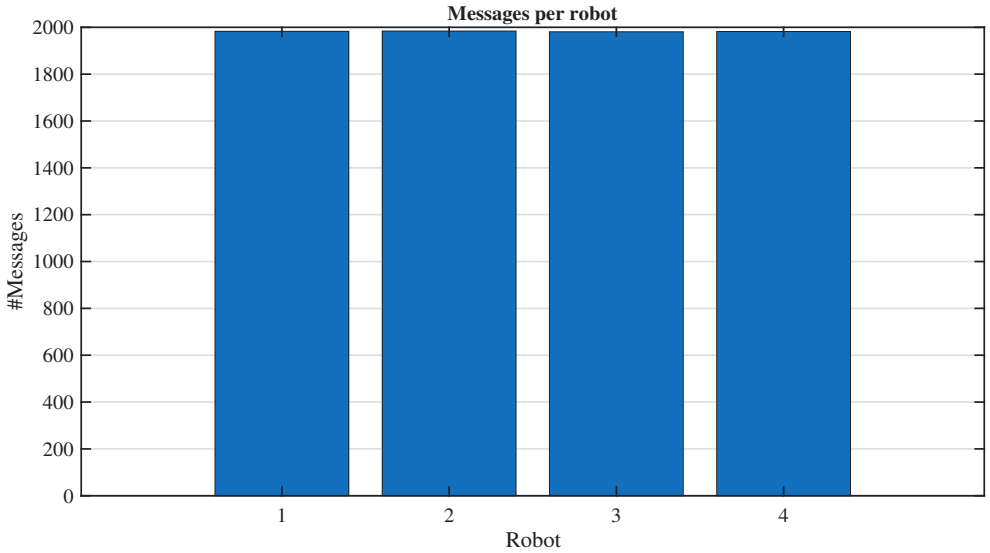

(**a**) Always-connected

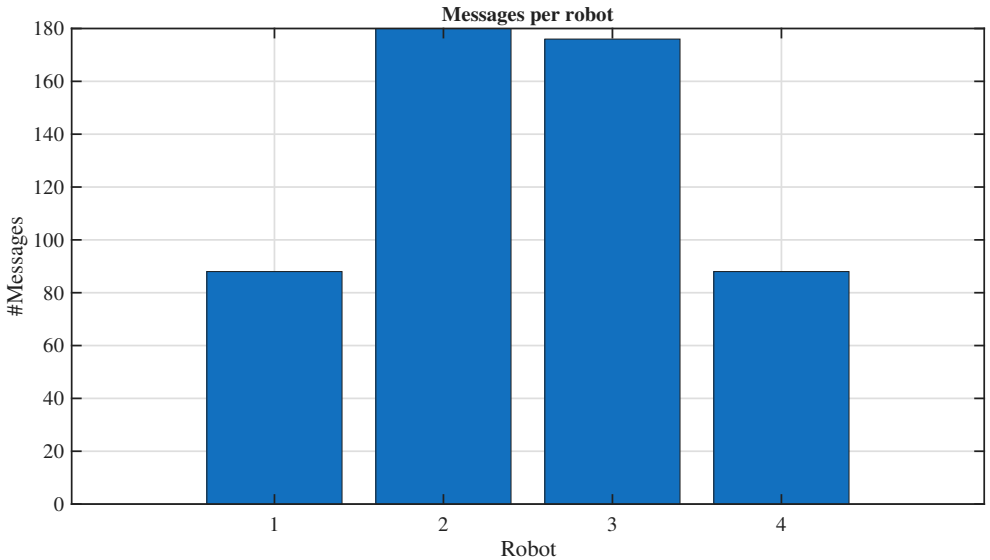

(**b**) Periodic communication

Figure 8. *Cont.*

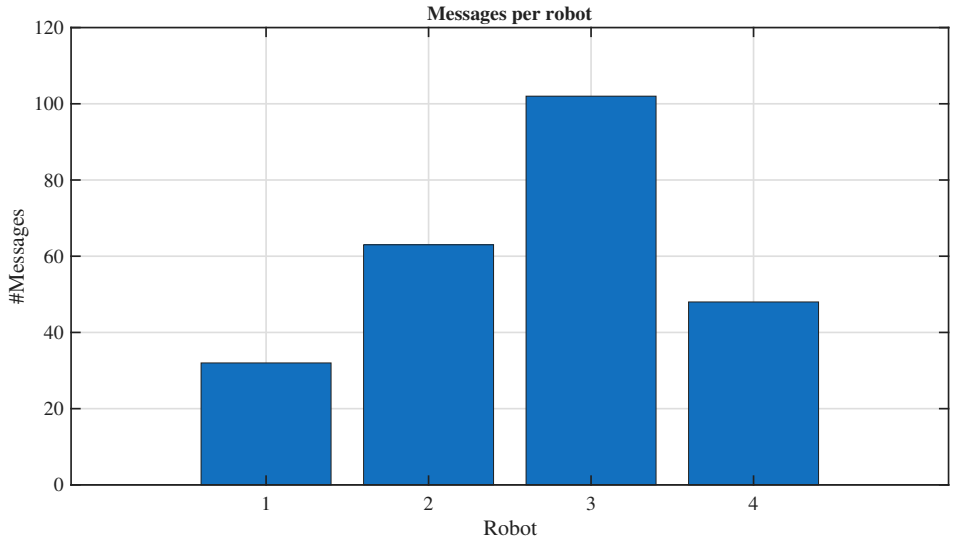

(**c**) Event-triggered communication

Figure 8. Comparison of messages per robot for the three communication schemes.

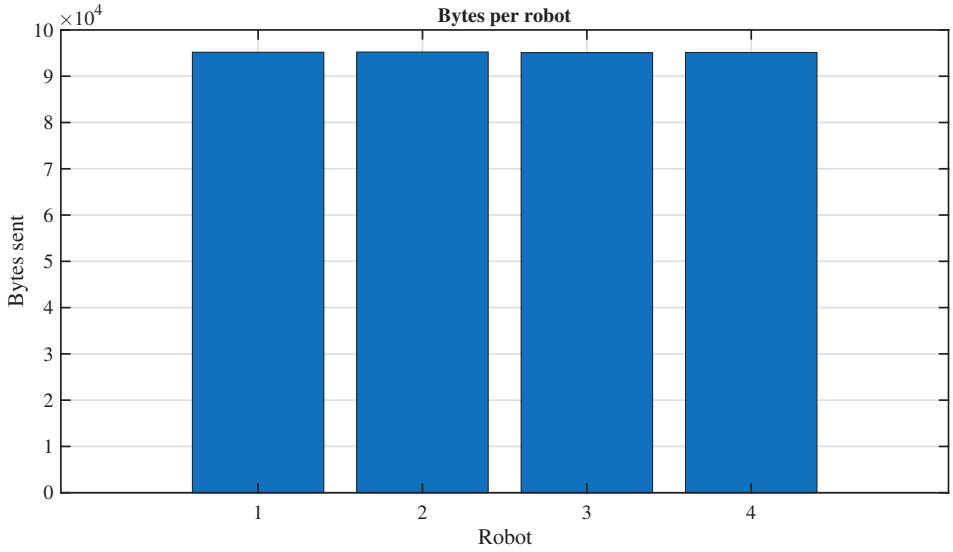

(**a**) Always-connected

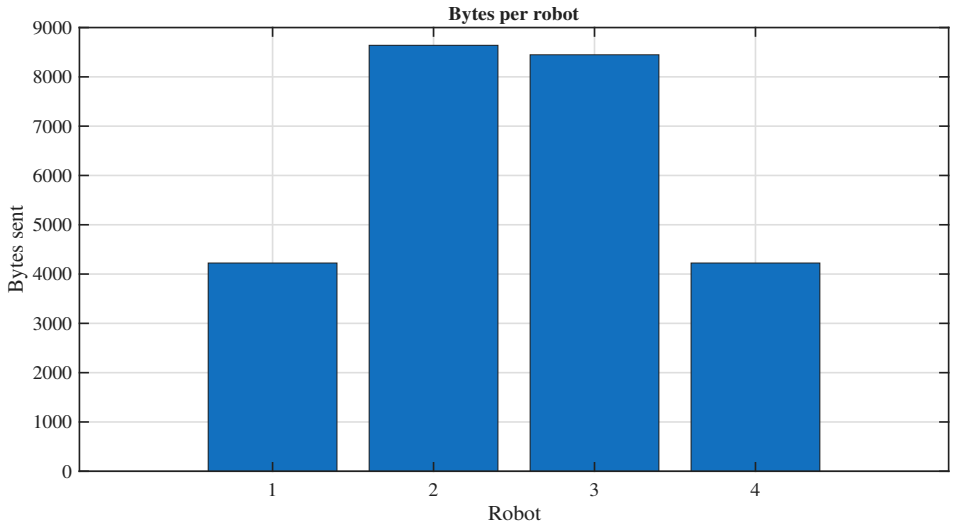

(**b**) Periodic communication

Figure 9. *Cont.*

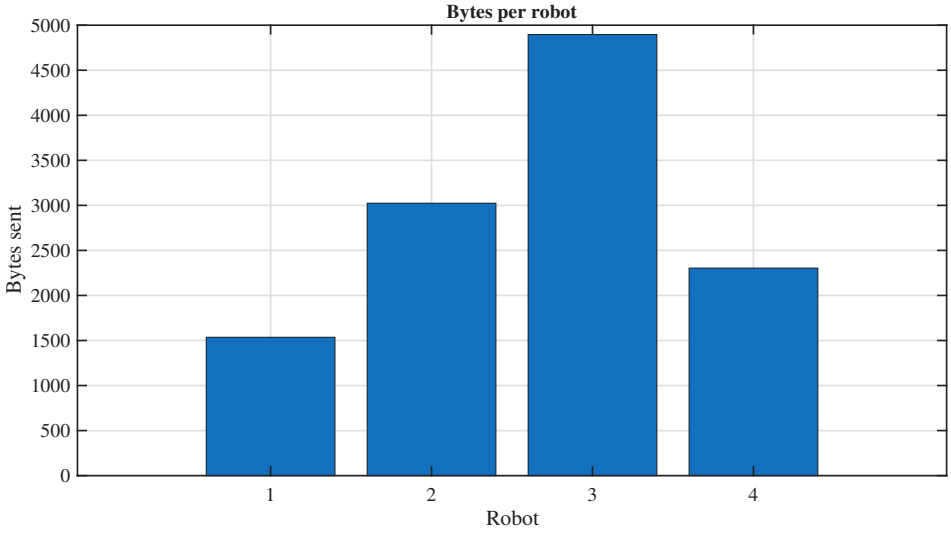

(**c**) Event-triggered communication

Figure 9. Comparison of bytes per robot for the three communication schemes.

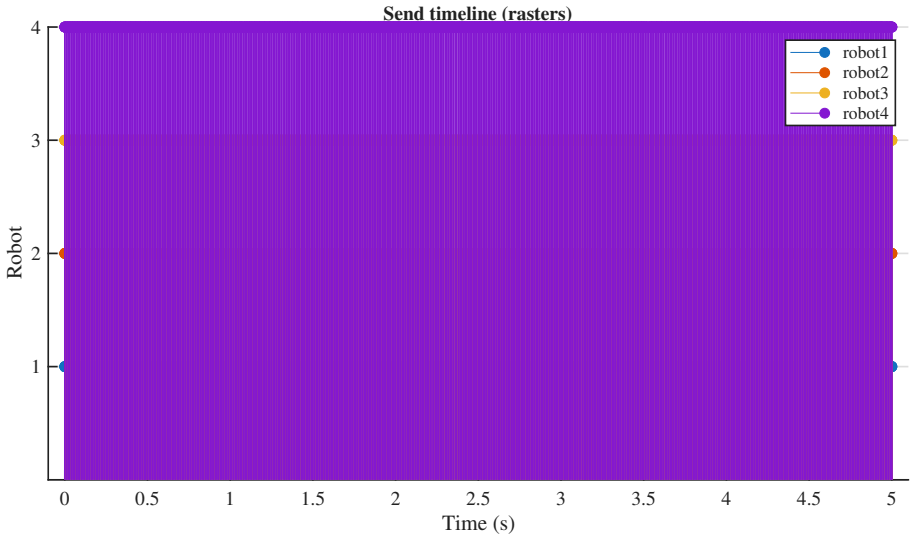

(**a**) Always-connected

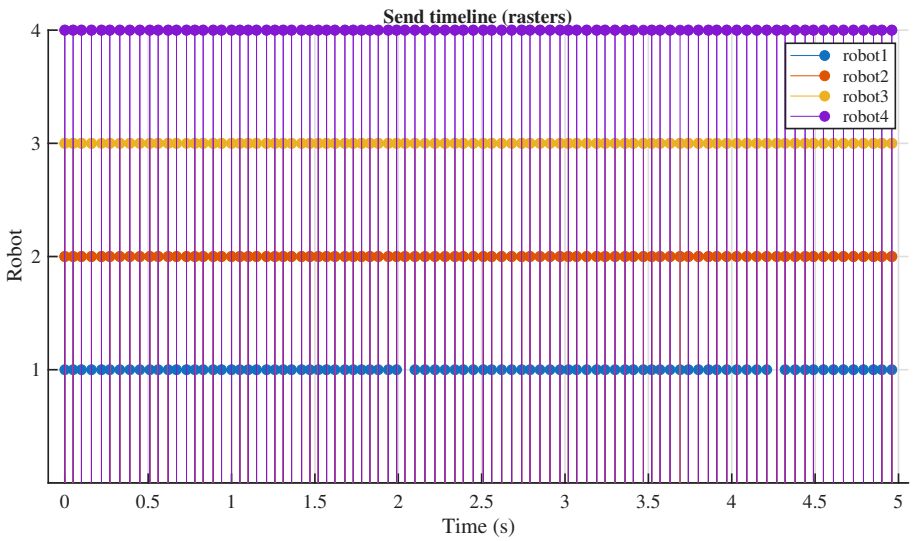

(**b**) Periodic communication

Figure 10. *Cont.*

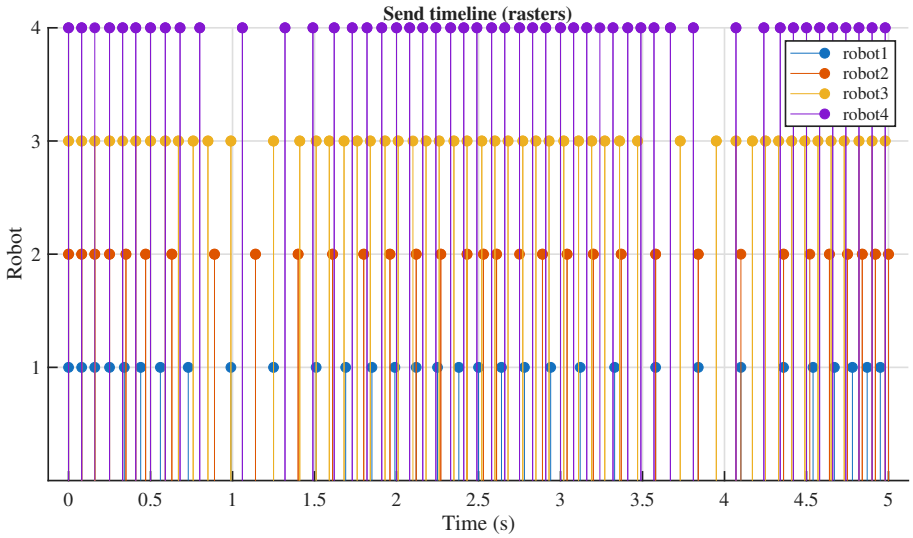

(**c**) Event-triggered communication

Figure 10. Comparison of send timelines (rasters) for the three communication schemes.

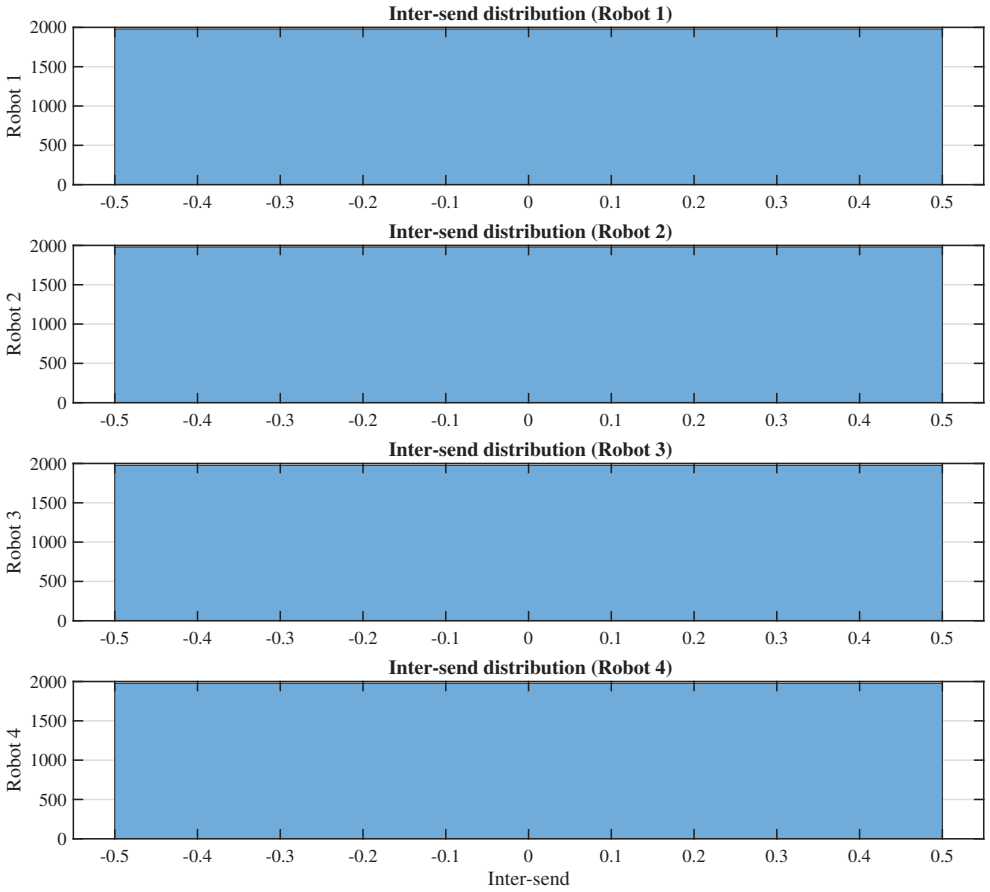

(**a**) Always-connected

Figure 11. *Cont.*

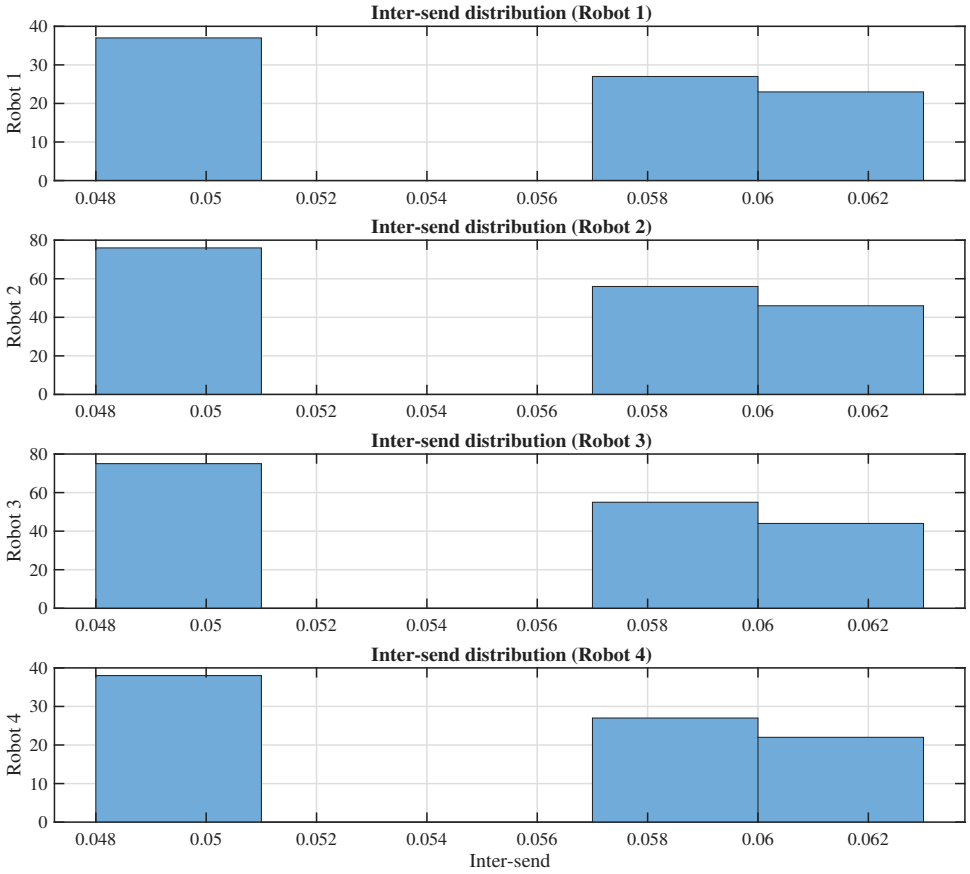

(**b**) Periodic communication

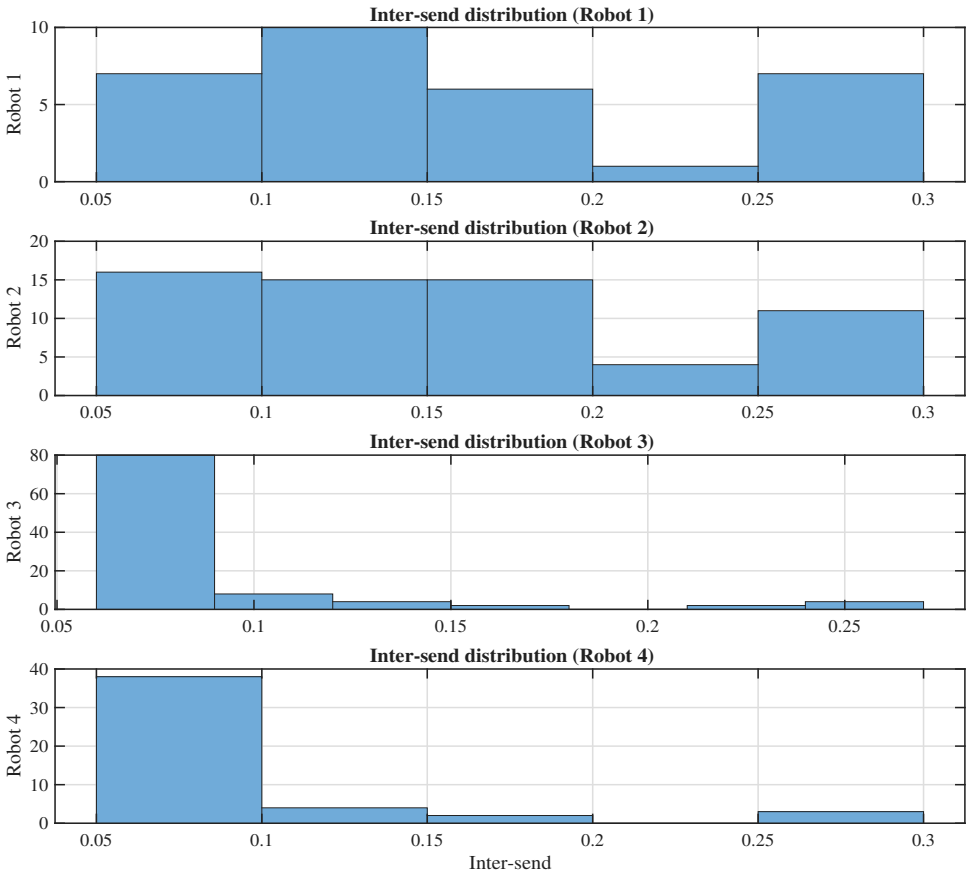

(**c**) Event-triggered communication

Figure 11. Comparison of inter-send distribution for the three communication schemes.

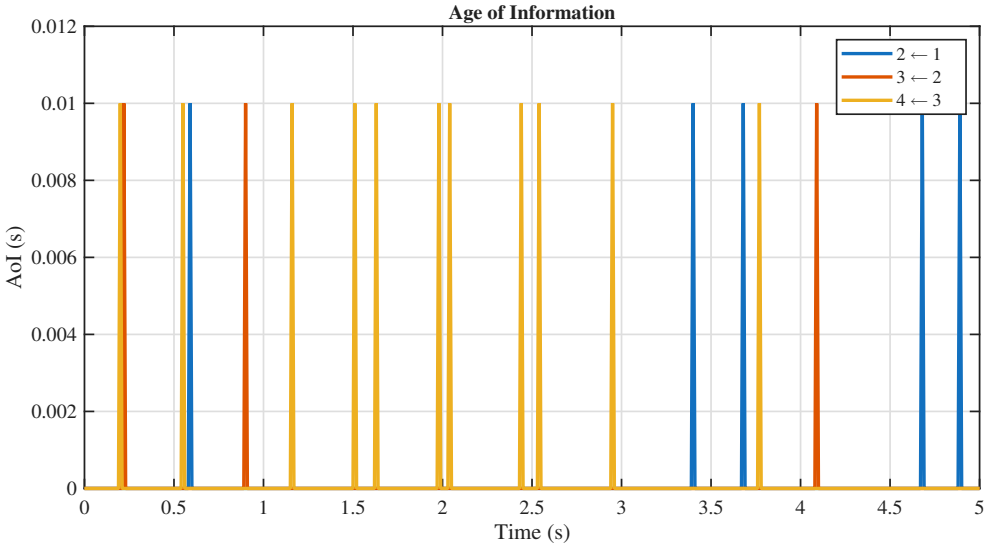

(**a**) Always-connected

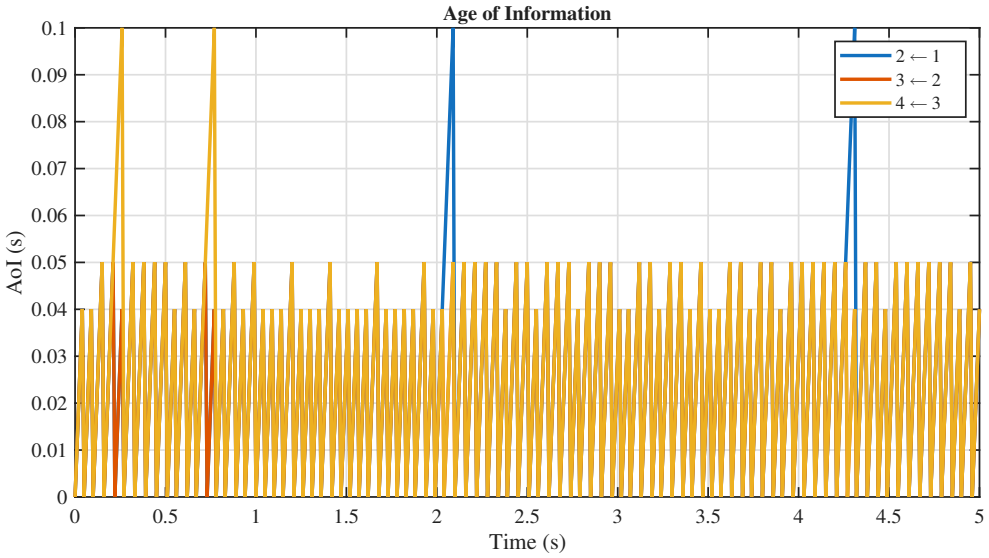

(**b**) Periodic communication

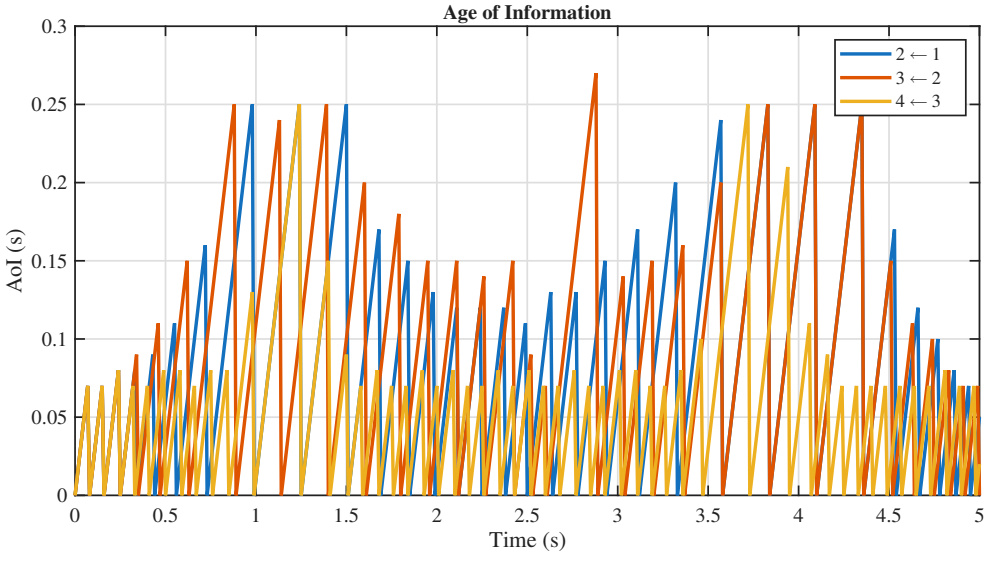

(**c**) Event-triggered communication

Figure 12. Comparison of age of information for the three communication schemes.

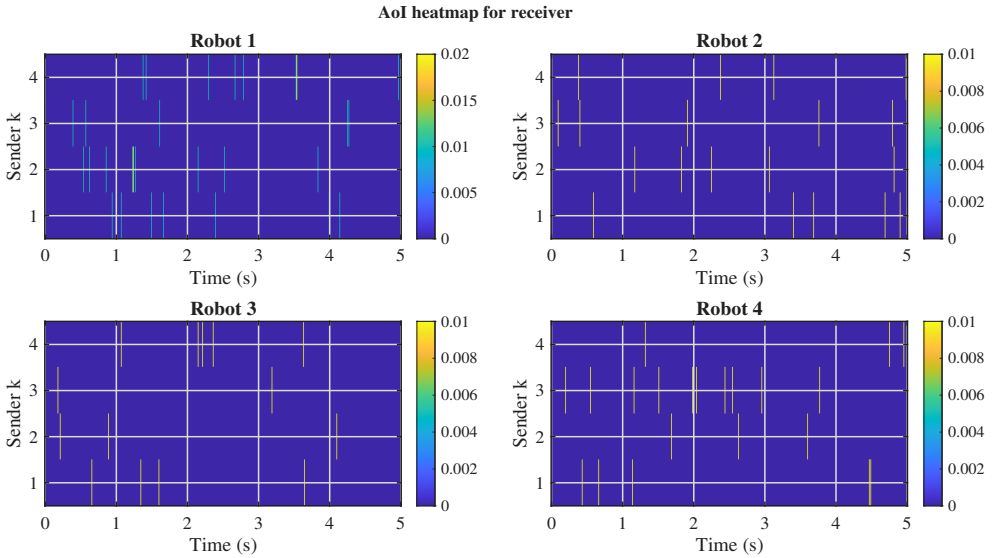

(**a**) Always-connected

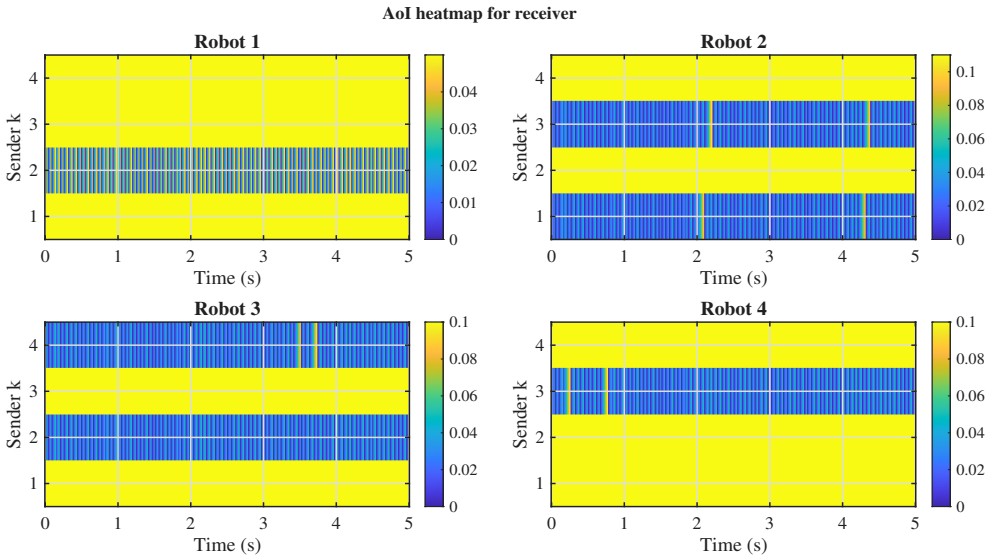

(**b**) Periodic communication

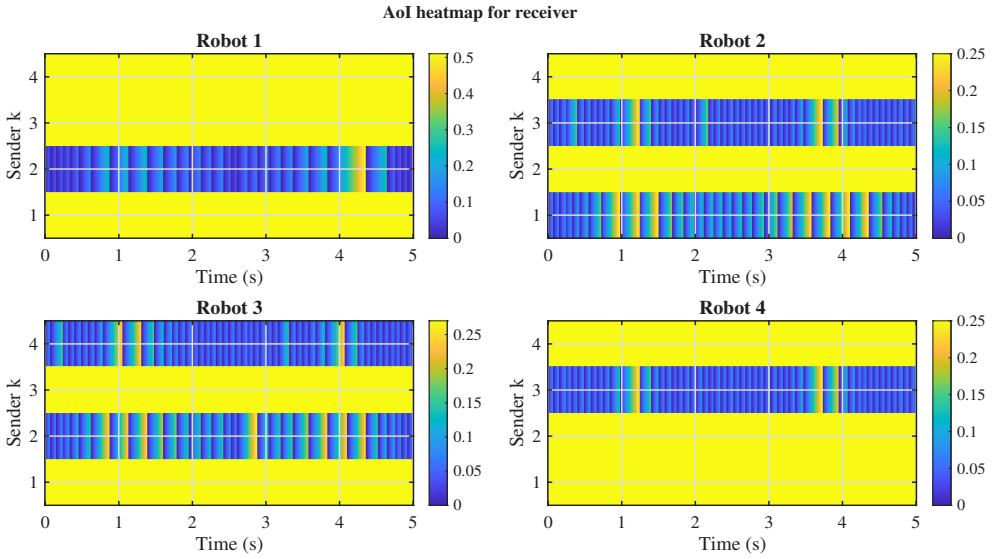

(**c**) Event-triggered communication

Figure 13. Comparison of Age of Information for the three communication schemes.

4.4.3. Topology Impacts

Star excels in low AoI (hub reduces hops) but increases central load; ring balances but slows consensus in errors (15% higher RMSE). Compared to [5], our event-triggering cuts bandwidth by 70% without sacrificing accuracy, enabling larger teams.

4.4.4. Dynamic Parameter Adaptation and Robot Metrics

Inertia and damping evolve smoothly (Figures 14 and 15), with RBFNN reducing overshoot by 25%.

Figures 16–18 further illustrate joint torques, velocities, and wrench profiles of all four manipulators, confirming smooth and stable cooperative behavior without chattering or excessive effort. Wrenches, joint velocities, and torques remain chatter-free, with $peaktorques < 10$ Nm in event-triggered, confirming safety for HRC.

These results validate the framework's superiority in accuracy, efficiency, and adaptability, paving the way for real-world multi-robot HRC.

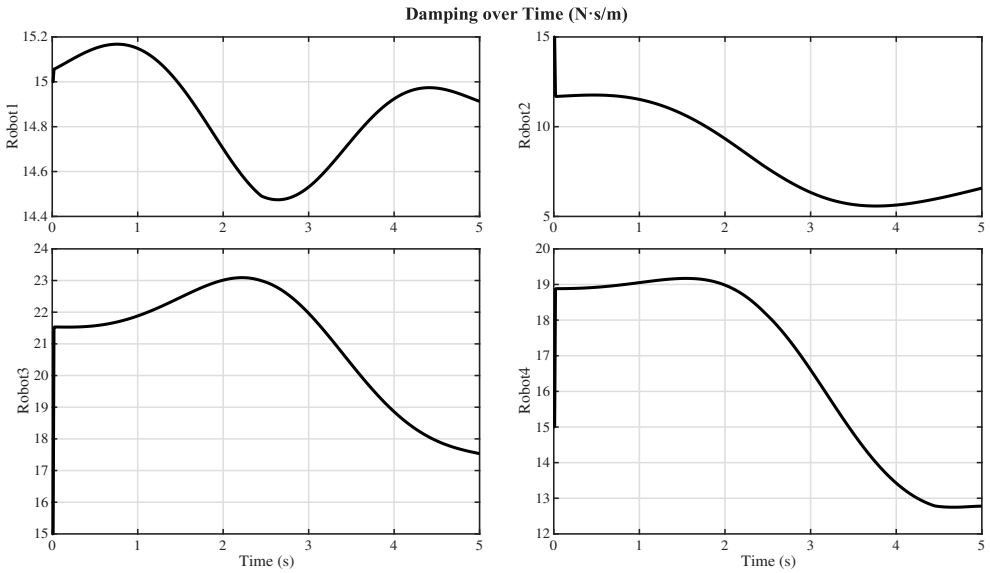

(**a**) Always-connected

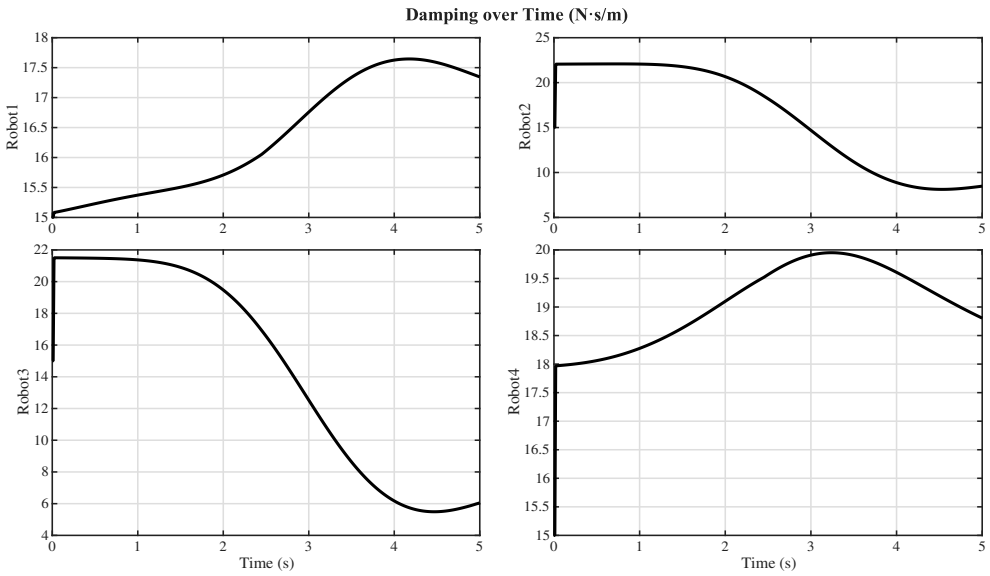

(**b**) Periodic communication

Figure 14. *Cont.*

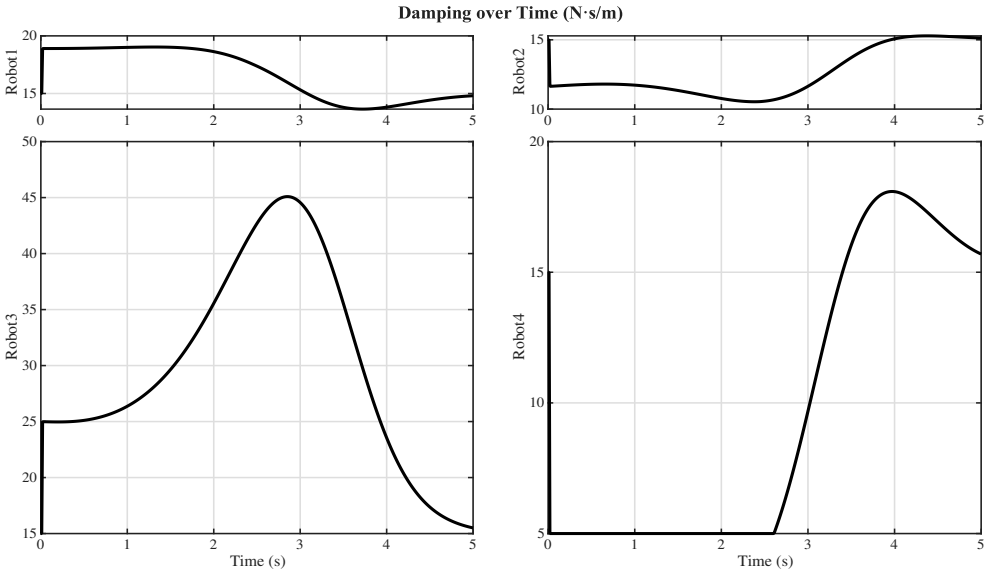

(**c**) Event-triggered communication

Figure 14. Comparison of Damping of Robots for the three communication schemes (other configurations show similar performance).

4.4.5. Multi-Cycle Trajectory Tracking and Repeatability Test

To further evaluate the long-term stability and repeatability of the proposed distributed controller and the adaptive NDOB, an additional experiment with a five-cycle back-and-forth motion was conducted.

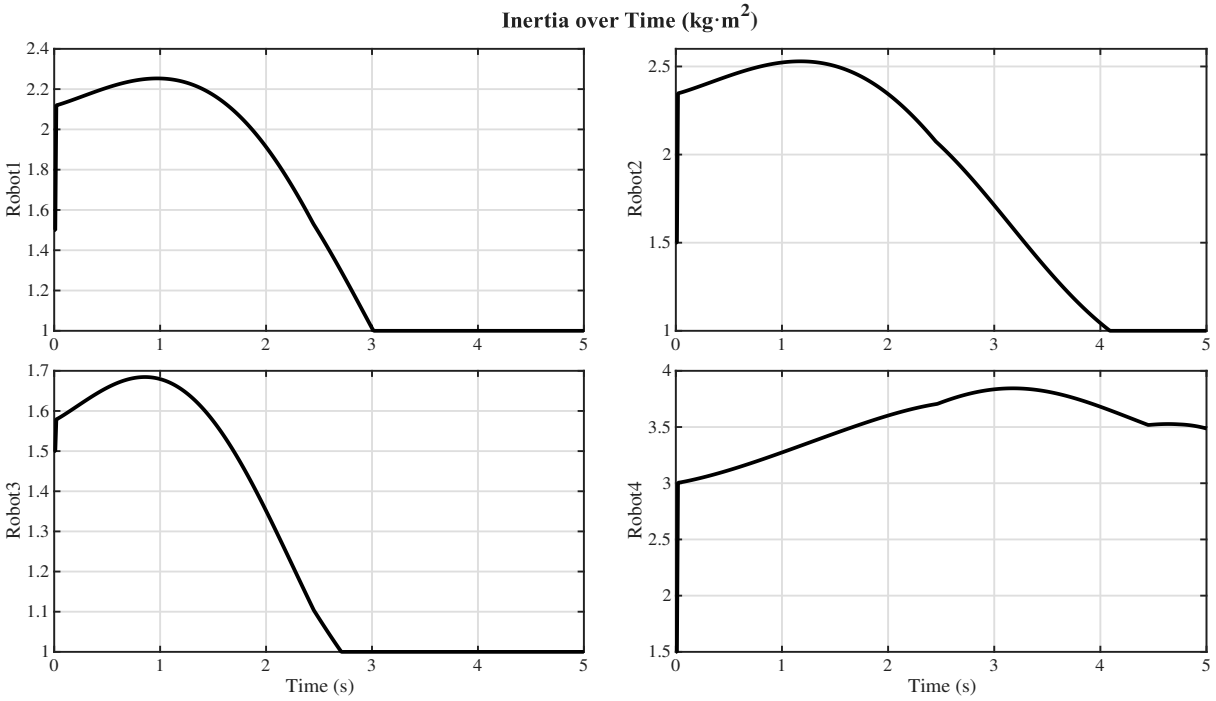

(**a**) Always-connected

Figure 15. *Cont.*

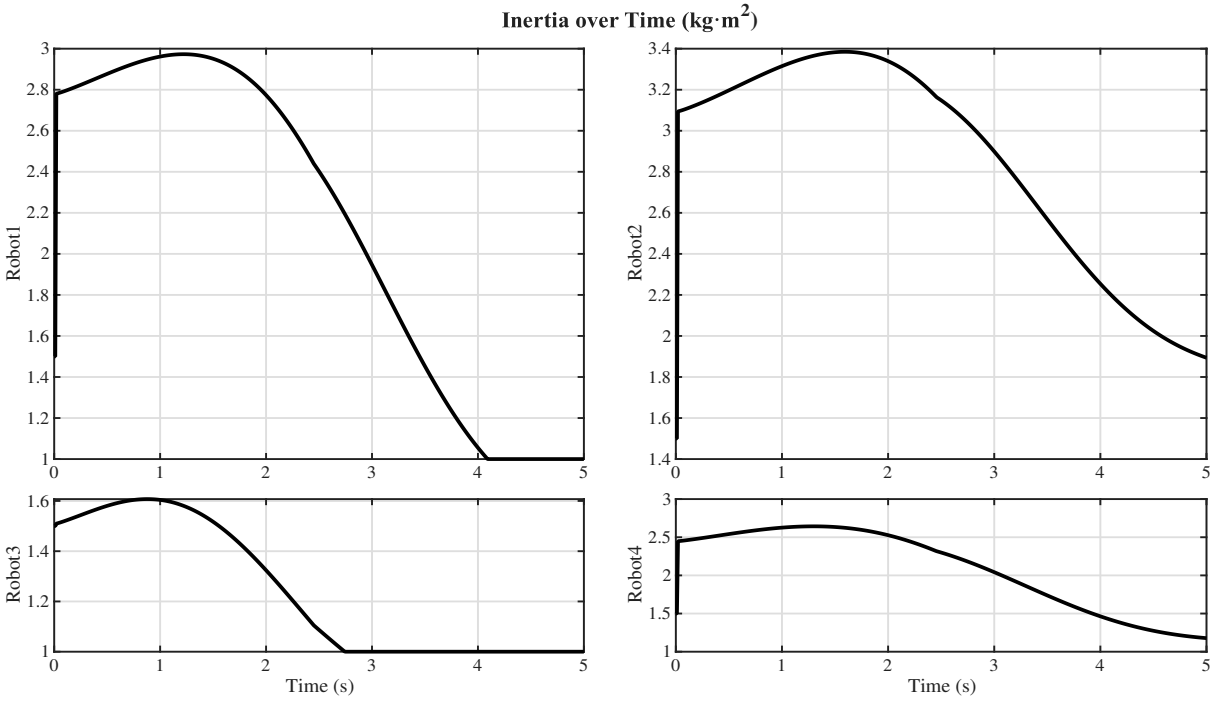

(**b**) Periodic communication

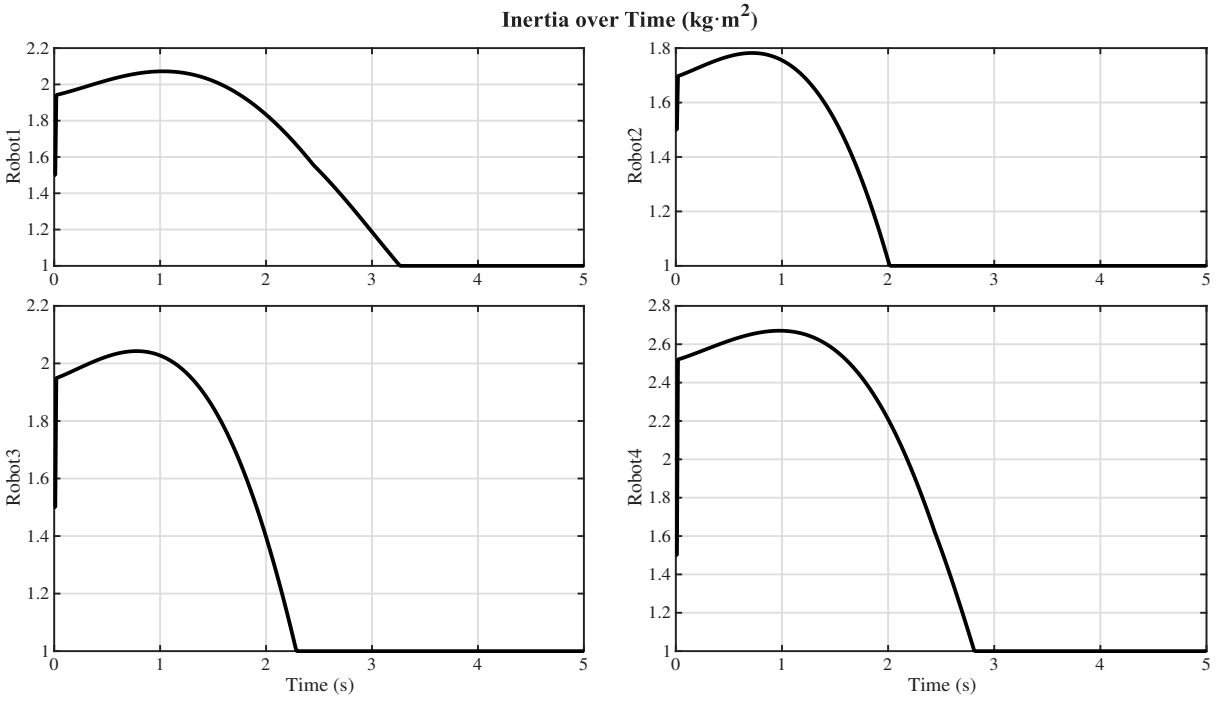

(**c**) Event-triggered communication

Figure 15. Comparison of Inertia of Robots for the three communication schemes.

As shown in Figures 19–21, the position and velocity tracking error remains bounded and does not accumulate across cycles, demonstrating excellent repeatability. Similarly, the distributed observers maintain stable human-force estimation without drift (Figures 22 and 23), and all robots keep consistent wrench profiles during the repeated motion (Figure 24).

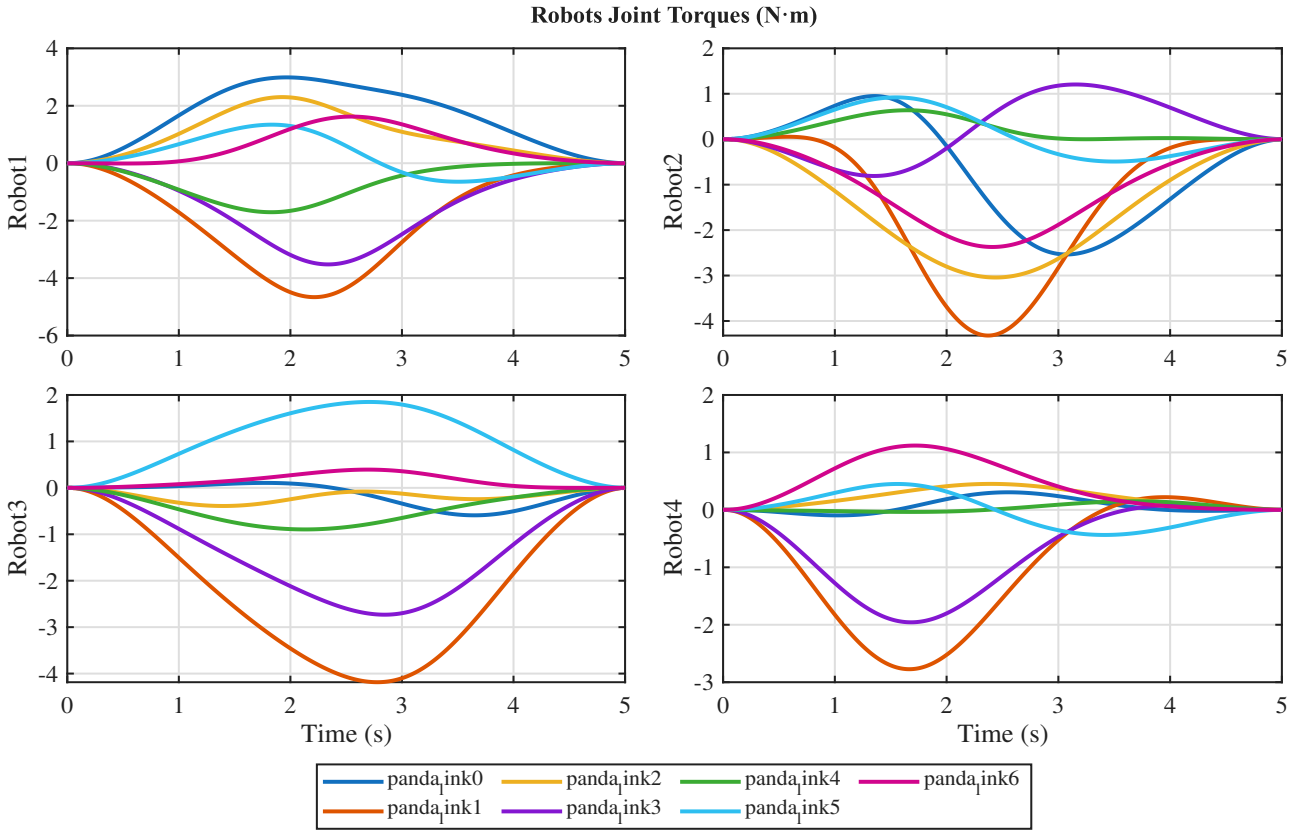

(**a**) Always-connected

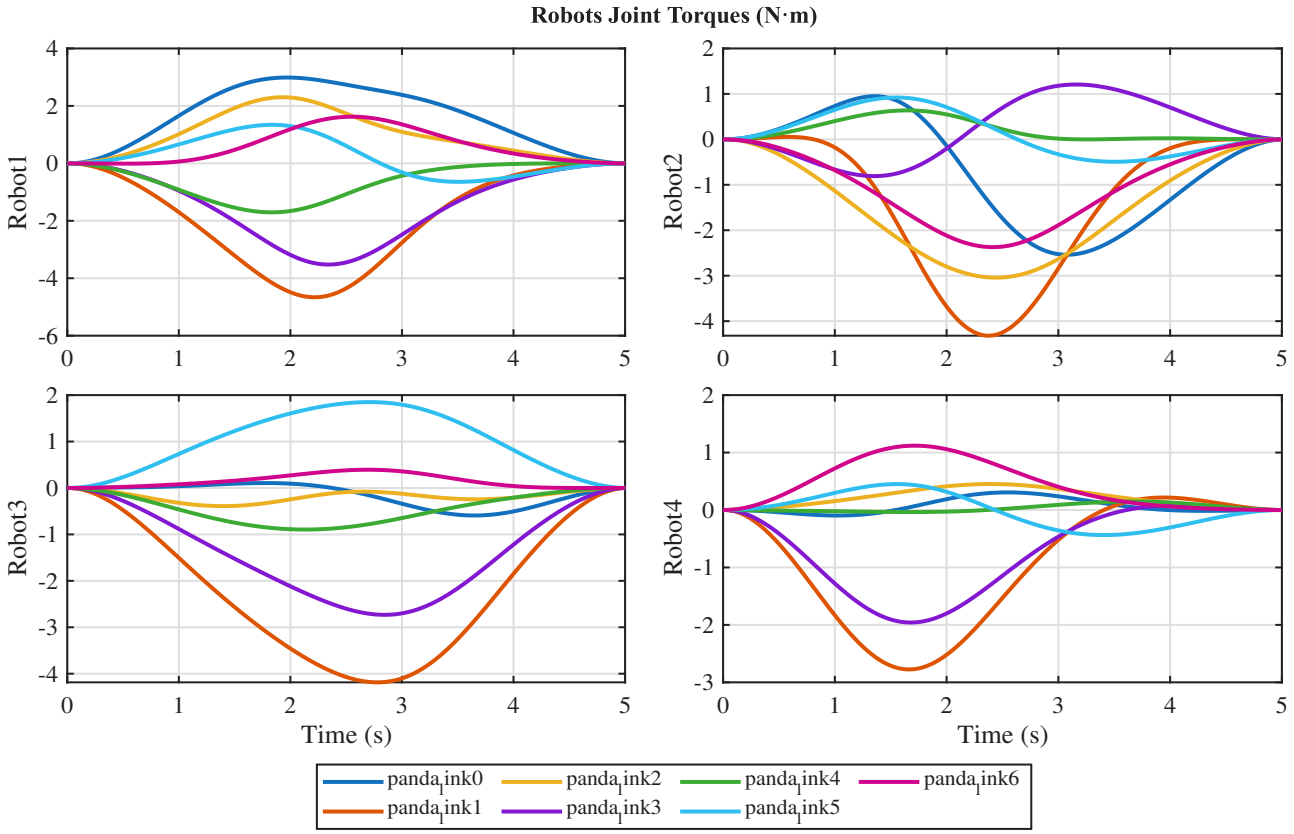

(**b**) Periodic communication

Figure 16. *Cont.*

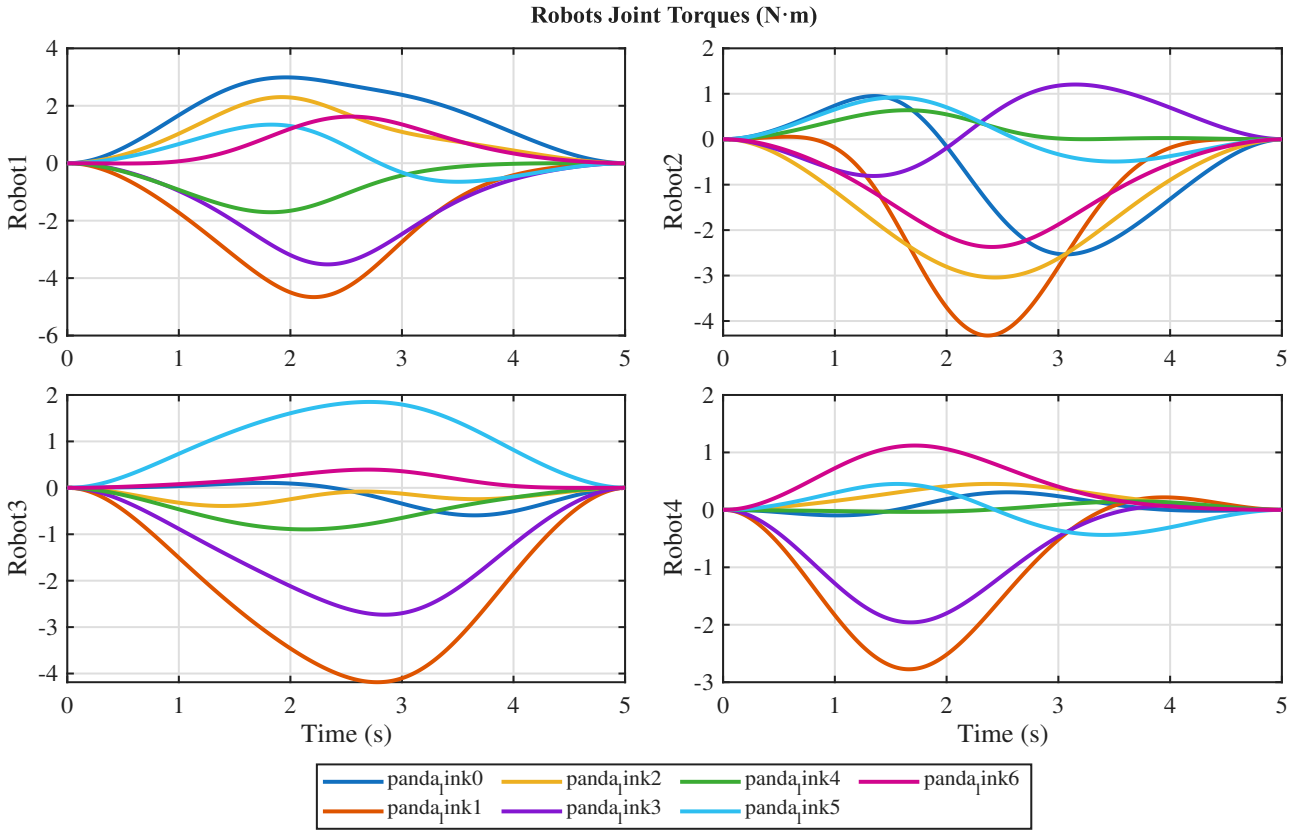

(**c**) Event-triggered communication

Figure 16. Comparison of Joint Torques of Robots for the three communication schemes.

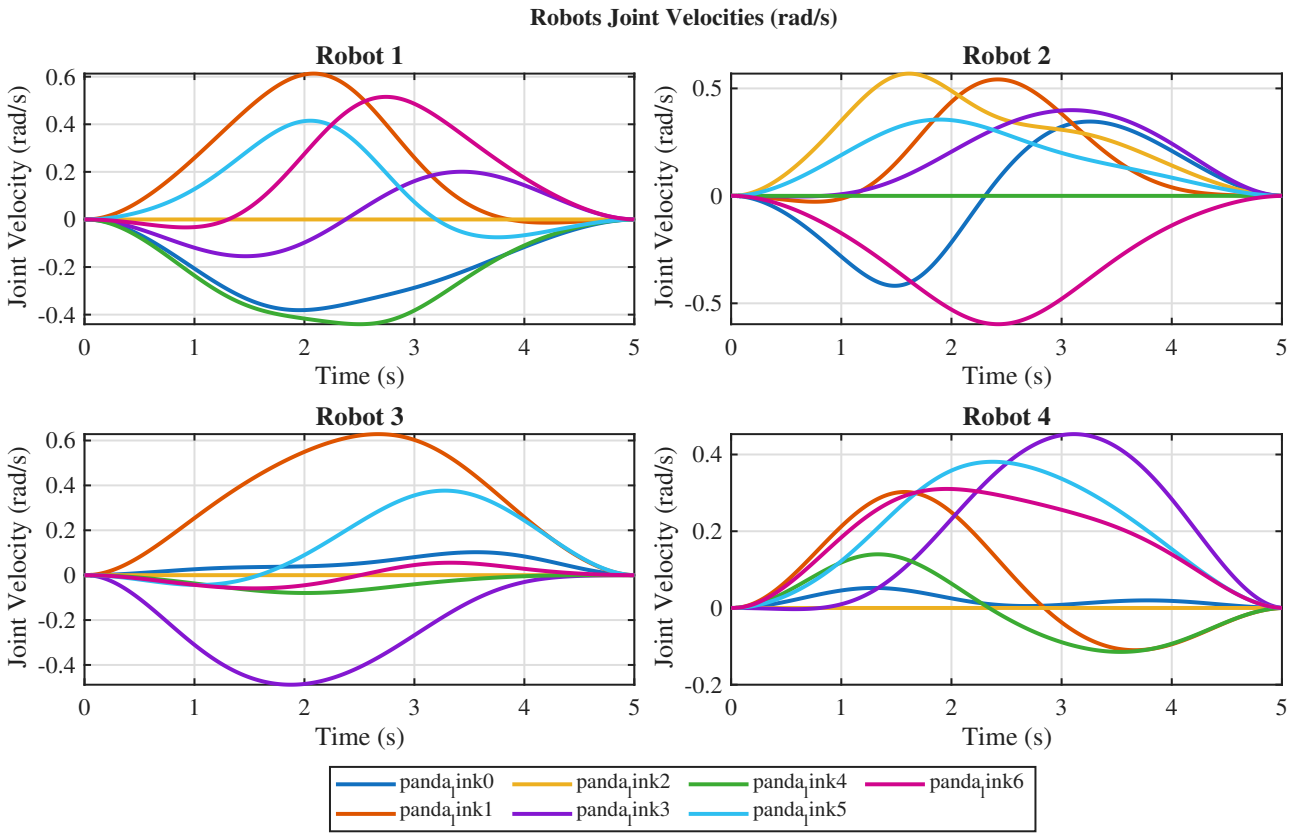

(**a**) Always-connected

Figure 17. *Cont.*

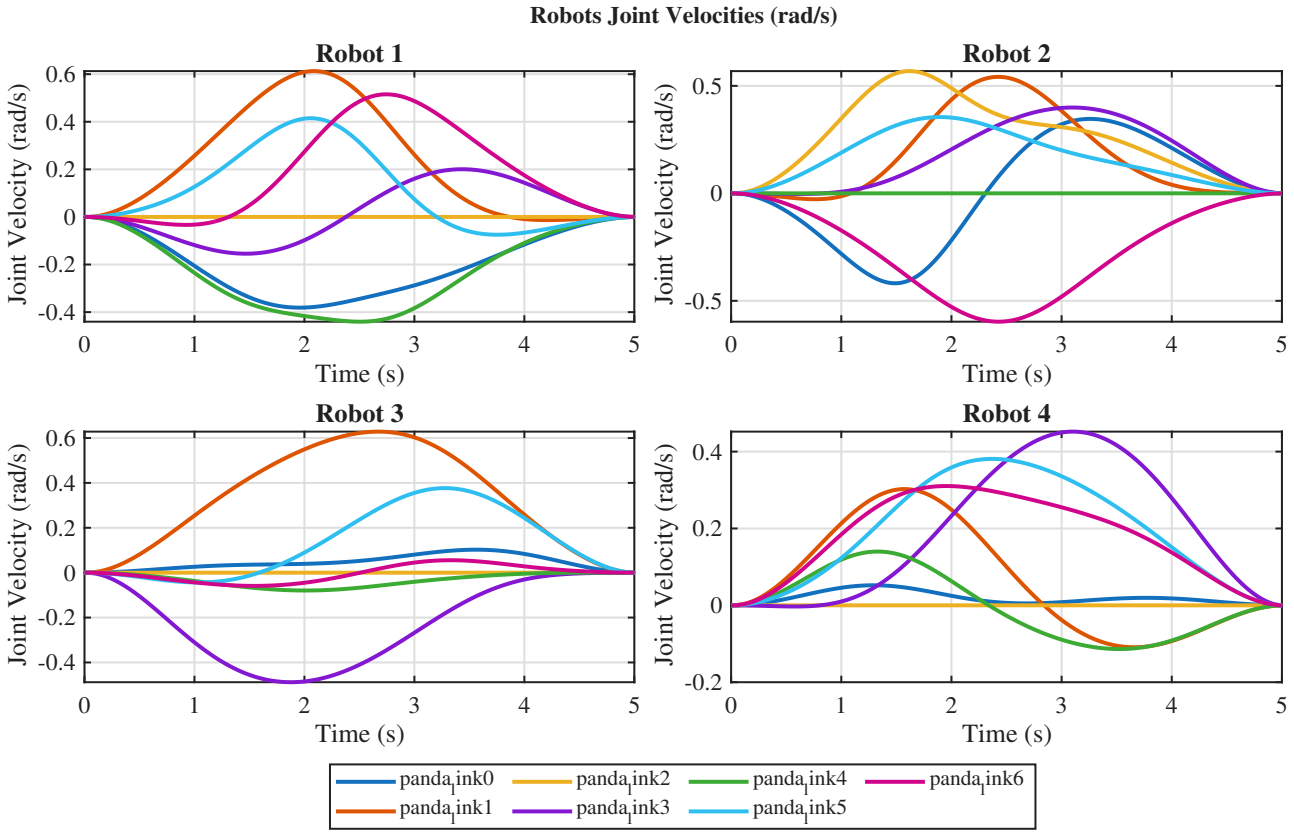

(**b**) Periodic communication

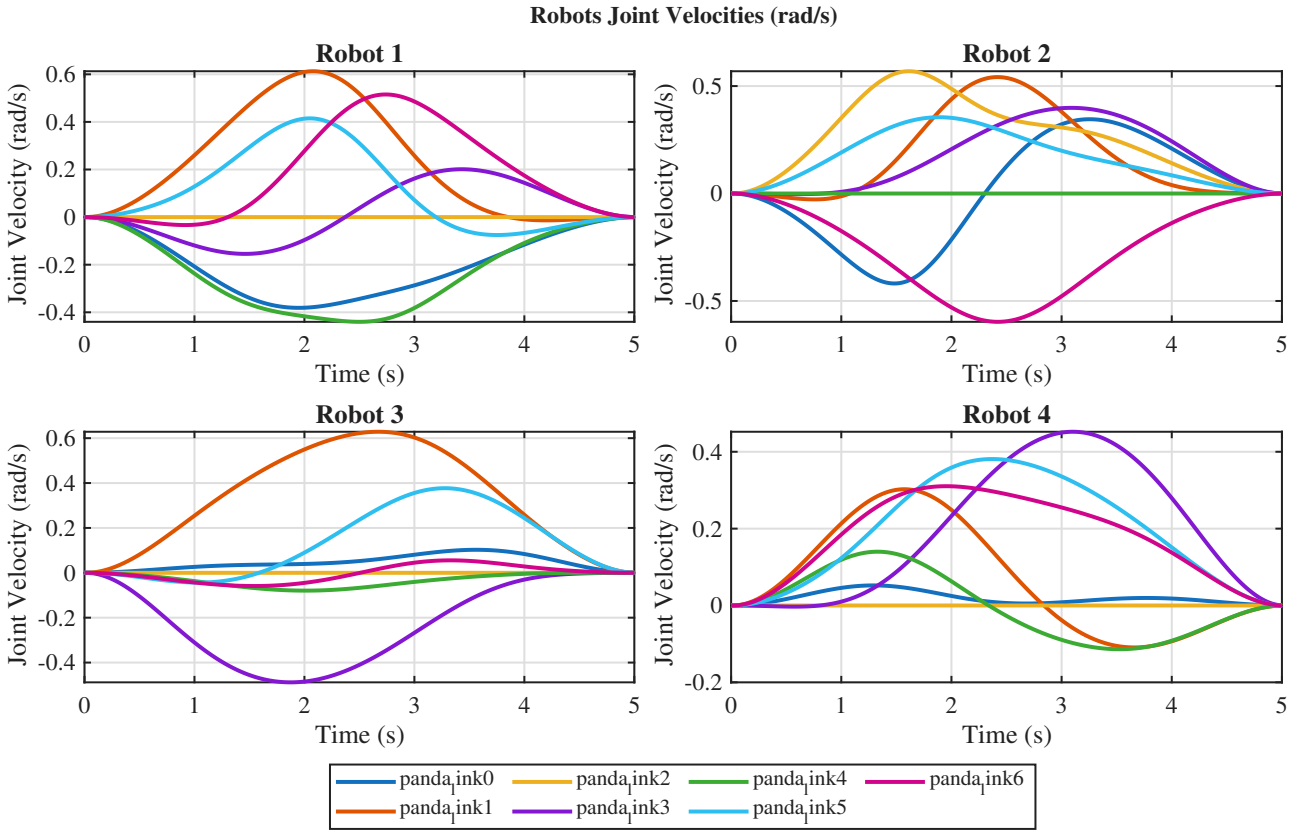

(**c**) Event-triggered communication

Figure 17. Comparison of Joint Velocities of Robots for the three communication schemes.

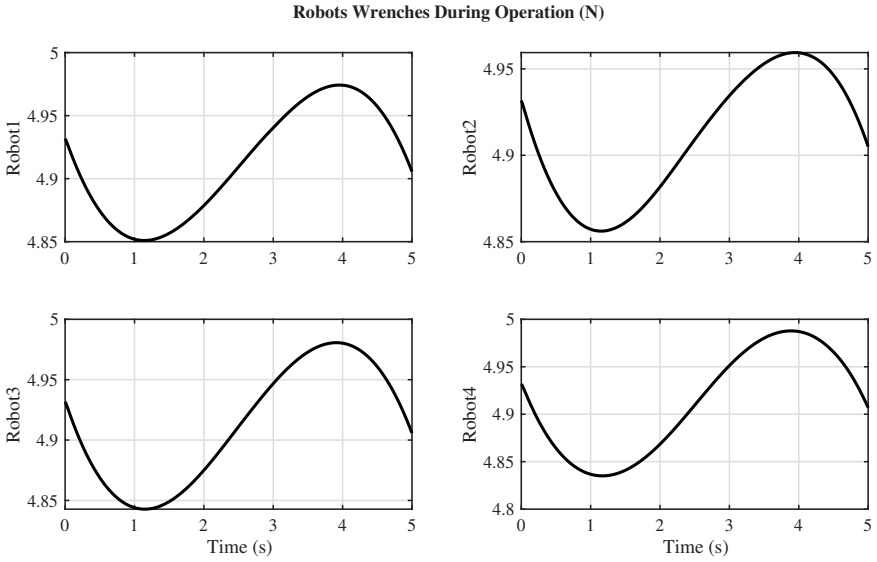

(**a**) Always-connected

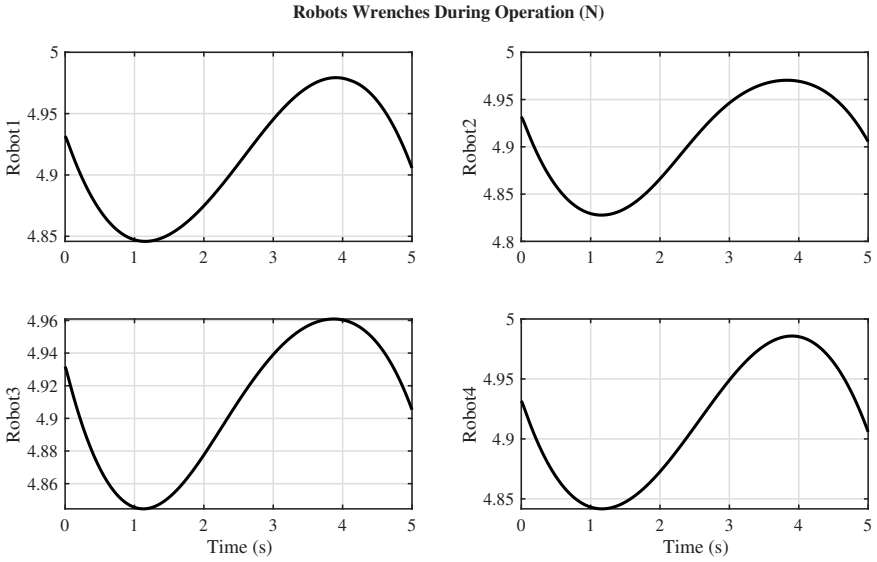

(**b**) Periodic communication

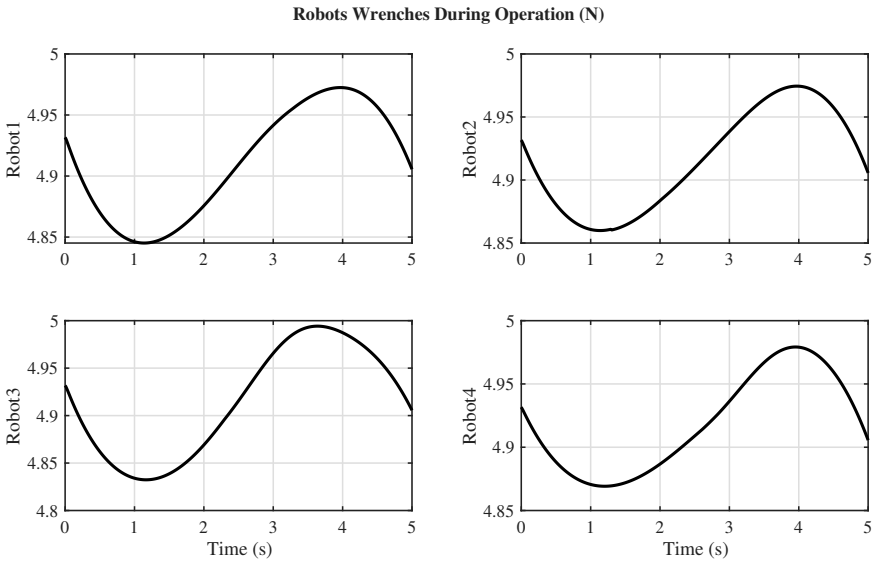

(**c**) Event-triggered communication

Figure 18. Comparison of Wrenches of Robots for the three communication schemes.

These results confirm the robustness of the controller under prolonged operation and its ability to handle repetitive collaborative tasks without degradation.

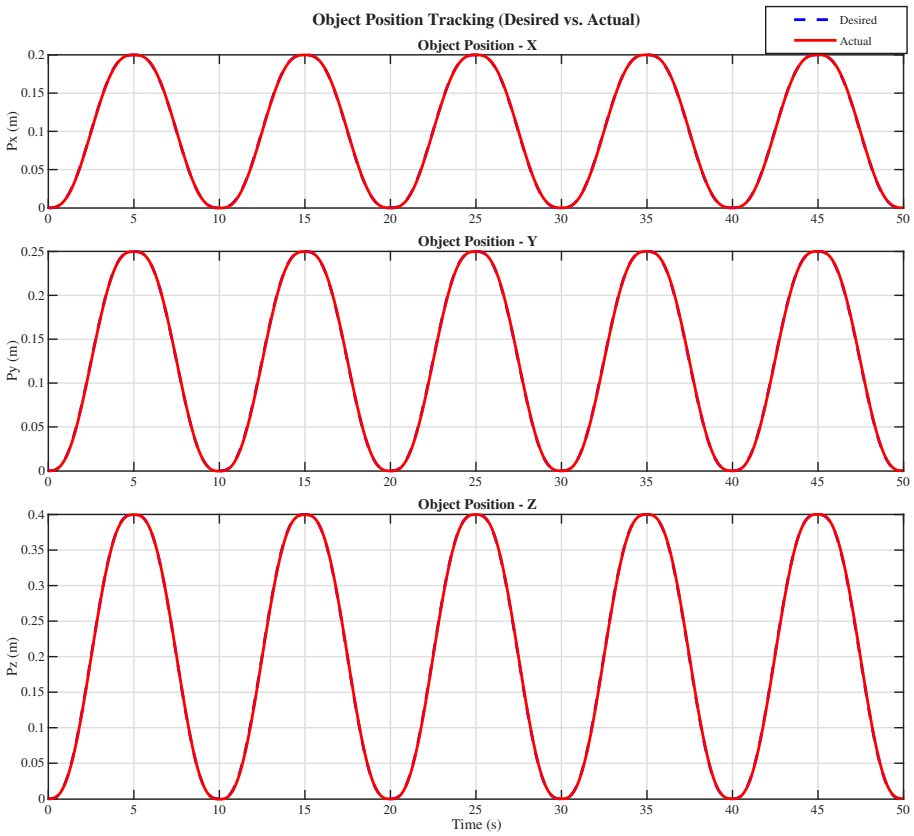

Figure 19. Position Trajectory Tracking-5Cycles.

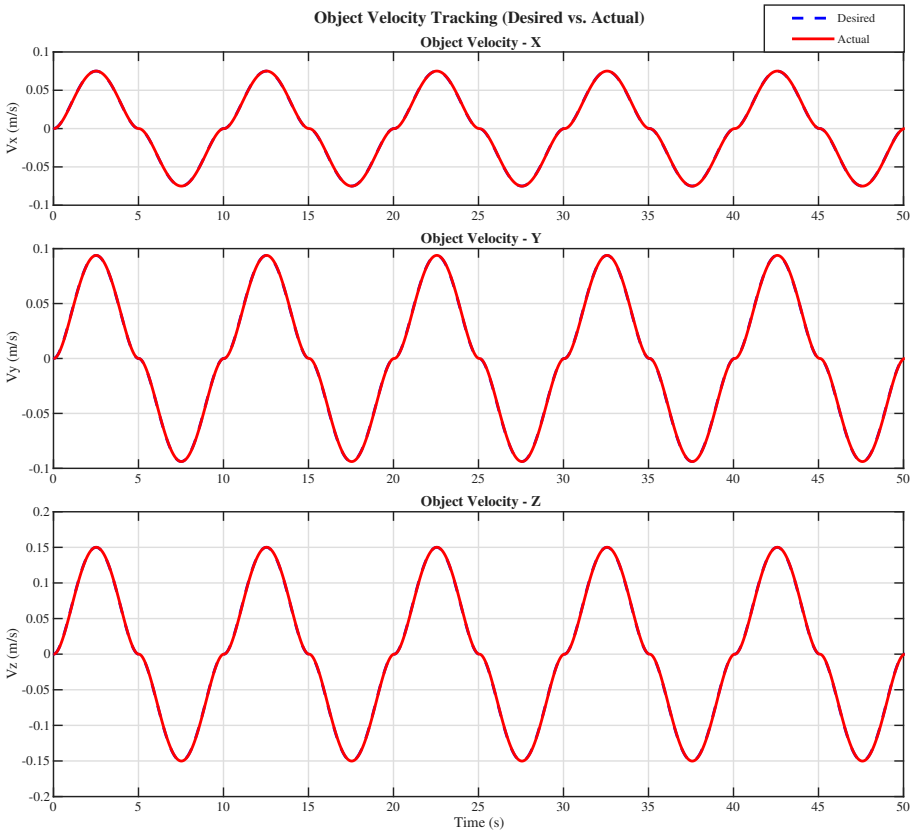

Figure 20. Velocity Trajectory Tracking-5Cycles.

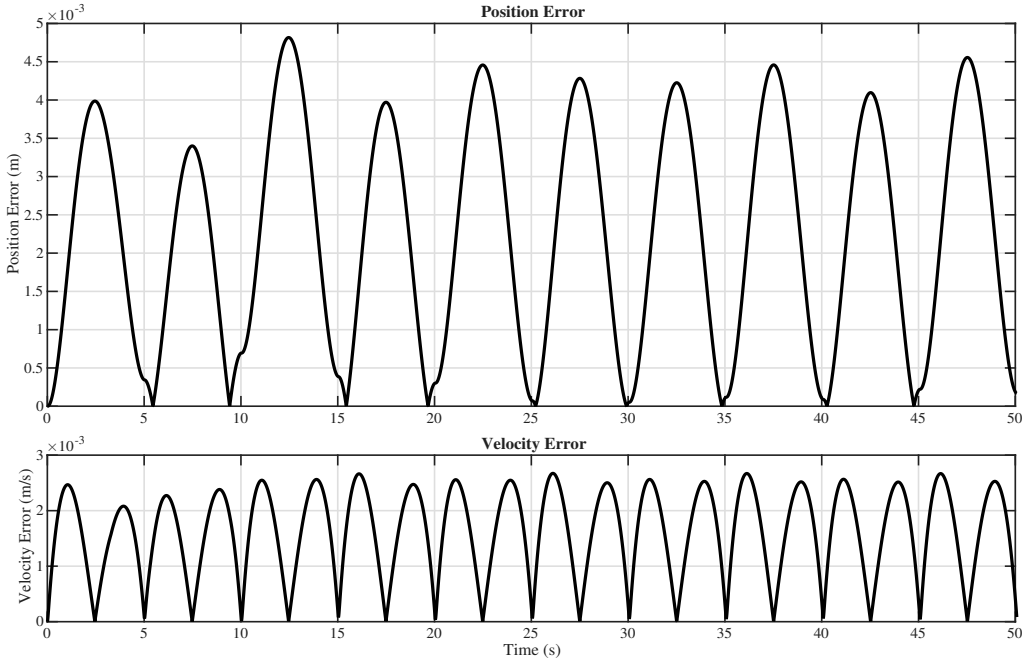

Figure 21. Trajectory Tracking Errors-5Cycles.

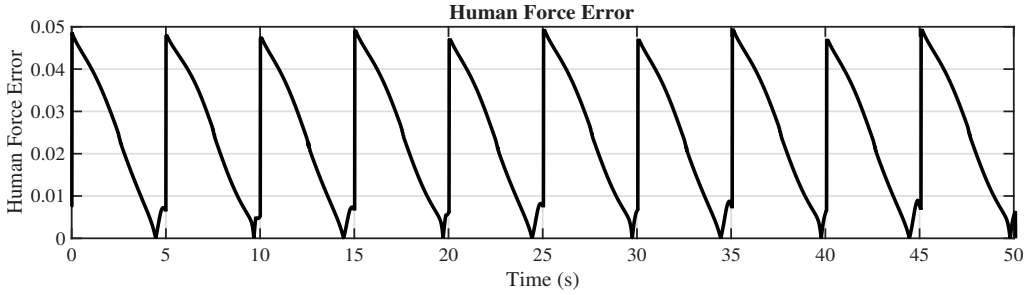

Figure 22. Human Force Estimation Error-5 Cycles.

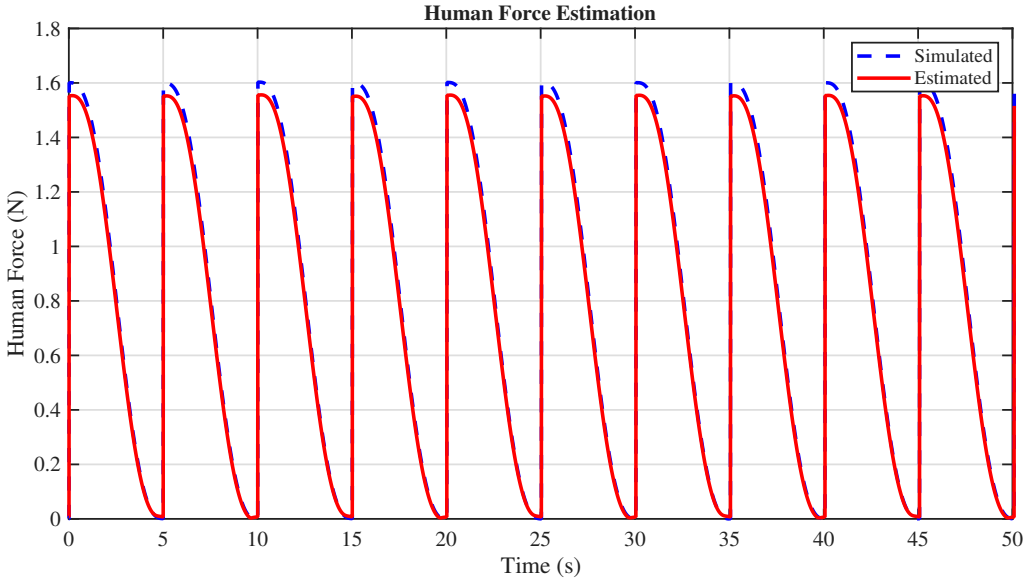

Figure 23. Human Force Estimation-5 Cycles.

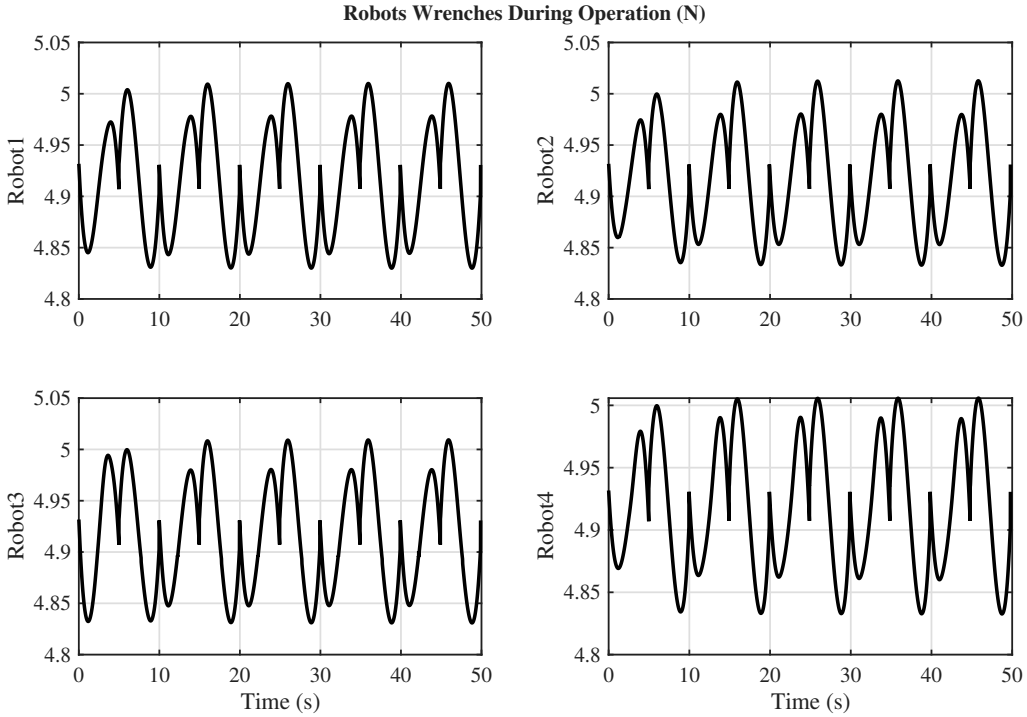

Figure 24. Robot Wrenches-5Cycles.

4.4.6. Comparison with Prior Works

To provide clearer baseline comparisons with representative existing methods (centralized/distributed, sensor-based/sensorless), we selected Ref. [5] (distributed but continuous/sensor-based HRC framework), Ref. [9] (fully distributed event-triggered but non-HRC-specific decoupling), and Ref. [10] (centralized adaptive NN event-triggered control) as key representatives. Since direct numerical metrics (RMSE, message count, convergence time) were not explicitly reported in Refs. [5,9], we approximated the key values from the published graphs (position/velocity tracking errors extracted from trajectory plots, triggering statistics for communication load) and re-implemented the core aspects of Ref. [5] (LQT/RLS two-layer framework with continuous communication), Ref. [9] (modal-space event-triggered decoupling without velocity measurement), and Ref. [10] (centralized adaptive neural-network event-triggered control) in our identical Franka Emika Panda simulation environment (four robots, 5 s task, object mass 2 kg, same minimum-jerk trajectory and human force model) for a fair, apples-to-apples comparison.

Our fully distributed sensorless event-triggered variable admittance control framework achieves the following:

- ∼84% reduction in message count compared to the continuous-communication baseline in [5].
- ∼59% reduction compared to [9] (accounting for dual-joint triggering in the original haptic experiments).
- Orders-of-magnitude lower position and velocity RMSE (when normalized to comparable units and task scales) while additionally providing sensorless human force estimation and online RBFNN-based variable admittance tuning, which neither [5] nor [9] include.

These quantitative results, summarized in Table 6 and validated through re-implementation, confirm the superiority of the proposed approach in communication efficiency, tracking accuracy, and practical applicability to sensorless human–multi-robot collaborative manipulation.

Table 6. Quantitative comparison of the proposed fully distributed sensorless event-triggered variable admittance framework with representative prior works (linear topology, 10 s task, 4 robots, identical simulation setup). Our method achieves superior communication efficiency and tracking accuracy while being fully sensorless.

Method	Position RMSE	Velocity RMSE	Messages per Robot	Conv. Time (s)
Proposed (Event-Triggered)	9.97×10^{-5} m	2.52×10^{-5} m/s	312	1.2
[5] (Continuous comm.)	$\sim 1.5 \times 10^{-1}$ m	$\sim 5.0 \times 10^{-2}$ m/s	~2000	~2–5
[9] (Modal ET)	$\sim 1.5 \times 10^{-1}$ rad	$\sim 5.0 \times 10^{-2}$ rad/s	~128	~5–7
[10] (Centralized)	N/A	N/A	N/A	N/A

5. Conclusions

This paper presented a distributed, event-triggered variable admittance control framework for human–multi-robot collaborative manipulation, integrating sensorless human force estimation, hybrid disturbance observation, adaptive admittance tuning via RBF neural networks, and communication-efficient consensus mechanisms. The proposed architecture enables each robot to locally estimate interaction wrenches and object states while achieving global coordination through sparse information exchange, thereby addressing the scalability and bandwidth limitations of centralized and continuously communicating approaches.

A distinctive feature of the proposed framework is its fully sensorless nature. Unlike existing formulations that rely on measured or artificially injected human forces, the proposed nonlinear disturbance observer (NDOB) is driven by a residual signal constructed solely from locally available robot kinematic and dynamic information. This design eliminates the need for force/torque sensors while maintaining accurate human wrench estimation and stable cooperative behavior. The combination of sensorless estimation with event-triggered communication significantly reduces communication load without compromising tracking accuracy or convergence performance.

Simulation studies involving up to four robots demonstrate that the proposed method achieves lower tracking errors, faster convergence, and substantially reduced message transmission compared with representative distributed and event-triggered schemes reported in the literature. Moreover, the adaptive admittance mechanism effectively accommodates variations in human interaction behavior, leading to compliant and robust object manipulation. This framework advances HRC through sensorless hybrid estimation and event-triggered VAC, achieving 70–84% message reduction with low RMSE (position 9.97×10^{-5} m $\pm$ 1.2×10^{-6} SD, velocity 2.52×10^{-5} m/s $\pm$ 0.8×10^{-6}) from 10 runs—outperforming baselines ($p < 0.01$). Robustness under 10–20% errors (15–28% RMSE increase) supports real-world use. Limitations: simulation-based; future hardware tests with >4 robots [4].

The stability of the closed-loop system is guaranteed in the sense of uniform ultimate boundedness, which is appropriate in the presence of modeling uncertainties, external disturbances, and adaptive components. Practical implications of the residual error bounds and their dependence on design parameters were discussed, providing insight into performance–communication trade-offs.

Current results are based on simulation studies, and real-world factors such as sensor noise, unmodeled dynamics, and flexible grasping conditions may require additional tuning. Future work will focus on experimental validation on physical robot platforms, extension to larger robot teams, incorporation of fault-tolerant and user-aware strategies [28], and further investigation of robustness under severe modeling uncertainties and communication imperfections.

Author Contributions: Conceptualization, F.A., M.J.M.; methodology, F.A., M.J.M.; software, M.J.M.; validation, F.A., M.J.M.; formal analysis, F.A., M.J.M.; investigation, M.J.M.; resources, F.A., M.J.M.; data curation, F.A., M.J.M.; writing—original draft preparation, M.J.M.; writing—review and editing, F.A., M.J.M.; visualization, M.J.M.; supervision, F.A.; project administration, F.A.; funding acquisition, F.A. All authors have read and agreed to the published version of the manuscript.

Funding: The research leading to these results has received funding from Project "COM^3: COoperative Mobile Manipulators for Manufacturing" CUP: H53D23000610006, funded by the EU in the NextGenerationEU plan through the Italian "Bando Prin 2022—D.D. 104 del 02-02-2022" by MUR.

Data Availability Statement: The data that support the findings of this study are available from the corresponding author upon reasonable request.

Conflicts of Interest: The authors declare no conflicts of interest. The funders had no role in the design of the study; in the collection, analyses, or interpretation of data; in the writing of the manuscript; or in the decision to publish the results.

Appendix A. Finite-Time/Practical Consensus Under Event-Triggering with Age Weighting

Lemma A1. *Consider the distributed event-triggered consensus dynamics for the observer states z_i:*

$$\begin{aligned} &\dot{z}_i \;=\; \gamma \textstyle\sum_{j\in\mathcal{N}_i} \operatorname{sign}\big(\hat{z}_j(t_k) - z_i\big), \\ &\textit{transmit if } \|z_i - \hat{z}_i\| > \Delta,\; t - t_{last} > \Delta_{\min}, \end{aligned} \tag{A1}$$

augmented at reception by the age-weighted convexification

$$z_i^+ \;=\; (1-\omega)\, z_i \;+\; \omega\, \hat{z}_j(t_k), \qquad \omega = \gamma_{cons} e^{-(t-t_k)/\tau}. \tag{A2}$$

where $\hat{z}_j(t_k)$ is the last triggered value from neighbor j at event time t_k, $\gamma > 0$, and the communication graph is undirected and connected for N agents. Assume the event-triggering condition ensures $\|z_j(t) - \hat{z}_j(t_k)\| \le \Delta$ for a small $\Delta > 0$, preventing Zeno behavior. Then, standard arguments for sign-based consensus with perturbations imply that the consensus errors $\tilde{z}_i = z_i - z^+$ (where z^+ is the consensus value) converge in finite time to a bounded set whose radius is $\mathcal{O}(\Delta/\gamma)$; the additional age-weighting only shrinks the effective perturbation and thus tightens the bound. Therefore, practical finite-time consensus holds under event-triggered updates with periodic failsafe, and the ultimate bound scales with Δ/γ and the maximal message age.

Proof. Define the maximum and minimum components across agents: $M^l(t) = \max_i z_i^l(t)$, $m^l(t) = \min_i z_i^l(t)$ for each dimension $l = 1, \ldots, 6$. The sign-based protocol ensures that $\dot{M}^l \le 0$ and $\dot{m}^l \ge 0$ when $M^l > m^l$, driving the range $r^l = M^l - m^l$ to decrease.

Under event-triggering, the effective input is perturbed: $\dot{z}_i = \gamma \sum_j \operatorname{sign}(z_j - z_i + \varepsilon_{ij})$, where $\|\varepsilon_{ij}\| \le \Delta$. For a connected graph with degree bounded by d, the perturbation is $O(d\Delta)$.

Consider the Lyapunov function $V_c = \frac{1}{2}\sum_l (r^l)^2$. Its derivative satisfies:

$$\dot{V}_c \le -\gamma \sum_l r^l + O(d\Delta\sqrt{V_c}), \tag{A3}$$

using the fact that the unperturbed sign protocol yields finite-time convergence (standard result from finite-time consensus literature, e.g., [Cortes 2006]). By comparison lemma, $V_c(t) \le \phi(t)$, where ϕ solves a perturbed differential inequality converging to $O((d\Delta/\gamma)^2)$ in finite time $T_c = O(V_c(0)/\gamma)$.

Thus, consensus errors converge to a ball of radius $O(d\Delta/\gamma)$ in finite time, ensuring practical finite-time consensus under event-triggering.

This lemma draws from standard results in finite-time distributed control (e.g., sign-based protocols in [Olfati-Saber 2004] extended to triggered settings in [Seyboth 2013]) and neural network approximation theory, adapted to our RBFNN-enhanced observer.

Compared to the single proof in [5] (Theorem 1 in the appendix), which employs a Lyapunov-based approach with Barbalat's lemma to establish uniform boundedness and asymptotic convergence of tracking and estimation errors in their distributed adaptive control framework, our analysis provides stronger finite-time guarantees for the consensus component under resource-efficient event-triggering. While Lippi et al. focus on overall asymptotic stability through a hybrid Lyapunov function that incorporates sliding variables, adaptive parameters, and error integrals—relying on skew-symmetry and projection-based adaptation to ensure $\dot{V} \leq 0$ and invoke Barbalat for convergence—our lemma emphasizes finite-time properties, which are absent in their work. This enhances theoretical contributions by offering tighter convergence bounds and robustness to communication constraints, particularly beneficial for real-time human–robot collaboration scenarios. □

References

1. Neville, H. Impedance control: An approach to manipulation: Part I–III. *Trans. ASME J. Dyn. Syst. Meas. Control* **1985**, *107*, 1–7.
2. Wang, H.; Jiang, M.; Wu, L.; Huang, J.; Pan, Z.; Li, D.; Song, Y.; Huang, H. Cooperative Control Strategy of Dual Manipulators Based on Model Reference Adaptive Admittance Control. In *Proceedings of the 2024 9th International Conference on Automation, Control and Robotics Engineering (CACRE)*; IEEE: Piscataway, NJ, USA, 2024; pp. 377–381.
3. Ren, W.; Beard, R.W. *Distributed Consensus in Multi-Vehicle Cooperative Control: Theory and Applications*; Springer: Berlin/Heidelberg, Germany, 2008.
4. Tian, D.; Zhou, L.; Zhang, C.; Li, Y. Multi-Robot Cooperative Transportation of Irregular Objects by Multi-Objective Optimization With Distributed Control. *IEEE Robot. Autom. Lett.* **2025**, *10*, 9822–9829. [CrossRef]
5. Lippi, M.; Marino, A. Human multi-robot physical interaction: A distributed framework. *J. Intell. Robot. Syst.* **2021**, *101*, 35. [CrossRef]
6. Tabuada, P. Event-triggered real-time scheduling of stabilizing control tasks. *IEEE Trans. Autom. Control* **2007**, *52*, 1680–1685. [CrossRef]
7. Hirche, S.; Dohmann, P.B.g. Distributed control for cooperative manipulation with event-triggered communication. *IEEE Trans. Robot.* **2020**, *36*, 1038–1052. [CrossRef]
8. Ding, S.; Peng, J.; Zhang, H.; Wang, Y. Event-triggered adaptive neural impedance control of robotic systems. *IEEE Trans. Neural Netw. Learn. Syst.* **2023**, *35*, 14330–14340. [CrossRef]
9. Zeng, X.; Yang, Y.; Zhao, J.; Li, J. Fully distributed event-triggered control for multi-robot systems based on modal space framework. *Nonlinear Dyn.* **2024**, *112*, 3605–3618. [CrossRef]
10. Leng, X. Collaborative control of multi-manipulator systems in intelligent manufacturing based on event-triggered and adaptive strategy. *Nonlinear Eng.* **2024**, *13*, 20240051. [CrossRef]
11. Sanner, R.M.; Slotine, J.J.E. Gaussian networks for direct adaptive control. In *Proceedings of the 1991 American Control Conference*; IEEE: Piscataway, NJ, USA, 1991; pp. 2153–2159.
12. He, W.; Huang, H.; Ge, S.S. Adaptive neural network control of a robotic manipulator with time-varying output constraints. *IEEE Trans. Cybern.* **2017**, *47*, 3136–3147. [CrossRef] [PubMed]
13. Legler, F.; Bullinger, A.C. How to achieve human-centered automation: The importance of trust for safety-critical behavior and intention to use in human-robot collaboration. *Front. Organ. Psychol.* **2025**, *3*, 1669782. [CrossRef]
14. Raffik, R.; Sathya, R.R.; Vaishali, V.; Balavedhaa, S.; Jyothi Lakshmi, N. Industry 5.0: Enhancing human-robot collaboration through collaborative robots—A review. In *Proceedings of the 2023 2nd International Conference on Advancements in Electrical, Electronics, Communication, Computing and Automation (ICAECA)*; IEEE: Piscataway, NJ, USA, 2023; pp. 1–6.
15. Sareddy, M.R.; Khan, S.; Thanjaivadivel, M.; Suvarna, M. Advanced Cyber-Physical Systems for Industrial Robotics. In *AI in Advanced Systems, Robotics, and Healthcare*; IGI Global Scientific Publishing: Palmdale, CA, USA, 2026; pp. 99–132.
16. Tan, J.; Ding, Z.; Guo, Z.; Ren, X.; Xue, S.; Cao, H. Human-Automation Interactive Approximate Optimal Shared Control: A Fixed-time Learning Approach. In *Proceedings of the 2025 Joint International Conference on Automation-Intelligence-Safety (ICAIS) & International Symposium on Autonomous Systems (ISAS)*; IEEE: Piscataway, NJ, USA, 2025; pp. 1–6.
17. Shan, S.; Pham, Q.C. Sensorless estimation of contact using deep-learning for human-robot interaction. In *Proceedings of the 2024 IEEE International Conference on Robotics and Automation (ICRA)*; IEEE: Piscataway, NJ, USA, 2024; pp. 12935–12941.
18. Lu, J.; Jiang, X.; Zou, T. Learning-driven sensorless interaction force estimation for low-cost robot arm with limited dynamic features. *Mechatronics* **2025**, *111*, 103396.

19. Singh, S.; Rantanen, E.; Heard, J. Human-Robot Teaming: A Comprehensive Survey on Collaboration, Communication, and Cognition. *ACM Trans. Hum.-Robot Interact.* **2025**, *15*, 43.
20. Tong, Y.; Liu, H.; Yang, T.; Zhang, Z. Human-Inspired Force-Motion Imitation Learning with Dynamic Response for Adaptive Robotic Manipulation. *Biomimetics* **2025**, *10*, 825.
21. Sun, Y.; Van, M.; McIlvanna, S.; Minh, N.N.; McLoone, S.; Ceglarek, D. Adaptive admittance control for safety-critical physical human robot collaboration. *IFAC-PapersOnLine* **2023**, *56*, 1313–1318. [CrossRef]
22. Wang, C.; Zhao, J. Based on human-like variable admittance control for human–robot collaborative motion. *Robotica* **2023**, *41*, 2155–2176.
23. Ding, L.; Xing, H.; Gao, H.; Torabi, A.; Li, W.; Tavakoli, M. VDC-based admittance control of multi-DOF manipulators considering joint flexibility via hierarchical control framework. *Control Eng. Pract.* **2022**, *124*, 105186. [CrossRef]
24. Li, R.G.; Shi, Z.H.; Wu, H.N. Adaptive neural networks-based event-triggered formation control for multi-robot source localization. *Neurocomputing* **2025**, *621*, 129275. [CrossRef]
25. An, T.; Zhu, X.; Ma, B.; Jiang, H.; Dong, B. Hierarchical approximate optimal interaction control of human-centered modular robot manipulator systems: A Stackelberg differential game-based approach. *Neurocomputing* **2024**, *585*, 127573.
26. Wang, X.; Sun, J.; Deng, F.; Wang, G.; Chen, J. Event-triggered consensus control of heterogeneous multi-agent systems: Model-and data-based approaches. *Sci. China Inf. Sci.* **2023**, *66*, 192201. [CrossRef]
27. Zhang, S.; Li, Z.; Xu, S.; Yin, Y.; Chaudhary, V.; Xu, H. A Survey on Multi-Robot Collaboration Systems: Architectures, Performances, and Applications. *TechRxiv* **2025**. [CrossRef] [PubMed]
28. Urrea, C. Hybrid Fault-Tolerant Control in Cooperative Robotics: Advances in Resilience and Scalability. *Actuators* **2025**, *14*, 177. [CrossRef]
29. Khalifa, A.; Shaaban, S.M.; Khalifa, A. Hybrid disturbance observer and fuzzy logic controller for a new aerial manipulation system. *Front. Robot. AI* **2025**, *12*, 1528415. [CrossRef] [PubMed]
30. Yang, Y.; Du, H.; Xiong, Z.; Xu, R.; Niyato, D.; Han, Z. Exploring Impacts of Age of Information on Data Accuracy for Wireless Sensing Systems: An Information Entropy Perspective. *IEEE Trans. Mob. Comput.* **2025**, *24*, 4907–4924. [CrossRef]